Construction and Building Materials 403 (2023) 133152

Contents lists available at ScienceDirect

Construction and Building Materials

journal homepage: www.elsevier.com/locate/conbuildmat

Study of the synergistic impact of Fe_3O_4, Na_2CO_3 and organic C on kaolin-based lightweight aggregates by a DOE (Mixture Experiments) approach

José Manuel Moreno-Maroto [a,b,*], Carlos Javier Cobo-Ceacero [b], Ana M. Martínez-Rodríguez [c], Antonio Conde-Sánchez [c], Beatriz González-Corrochano [b], Jacinto Alonso-Azcárate [d], Manuel Uceda-Rodríguez [b], Ana B. López [b], Carmen Martínez-García [b], Teresa Cotes-Palomino [b]

[a] Department of Geology and Geochemistry, Faculty of Sciences, Autonomous University of Madrid, Cantoblanco, 28049 Madrid, Spain
[b] University of Jaén. Department of Chemical, Environmental and Materials Engineering, Higher Polytechnic School of Linares, Scientific and Technological Campus of Linares, 23700, Linares (Jaén), Spain
[c] University of Jaén. Department of Statistics and Operations Research. Campus of Las Lagunillas, 23071, Jaén, Spain
[d] University of Castilla-La Mancha. Department of Physical Chemistry, Faculty of Environmental Sciences and Biochemistry, Avenida Carlos III, s/n, 45071 Toledo, Spain

ARTICLE INFO

Keywords:
Lightweight aggregate
Iron
Na_2CO_3
Organic carbon
Mixture Experiments

ABSTRACT

The compositional synergies involved in the thermal formation of lightweight aggregates (LWAs) have been investigated through four pure phases: non-expansive kaolin (K); cork powder (C); sodium carbonate (N) and magnetite-Fe_3O_4 (M). Mixture Experiments has been applied for formulation, modeling and optimization. LWAs have been manufactured from 36 starting mixtures and the main technological properties have been characterized: bloating index (*BI*), particle density (ρ_{rd}), water absorption (WA_{24}) and crushing strength (*S*). Maximum *BI* and WA_{24} together with minimum density are associated with the addition of a significant amount of iron phase in combination with small proportions of organic carbon (Optimal [BI > 60%]: 56.0% K + 40.2% M + 3.9% C + 0% N), while *S* increases antagonistically with expansion. Iron reduction by incomplete combustion of C appears to be critical in pore formation and concomitant bloating. N has enhanced the sphericity of the expanded specimens. The contrast between experimental and estimated data has shown that the models have generally performed very well.

1. Introduction

The term *aggregate* covers those granular materials whose application is fundamentally linked (although not exclusively) to the construction sector. Aggregate is, therefore, a highly strategic asset from an economic, social and environmental perspective [1,2]. From a regulatory standpoint, lightweight aggregate (LWA) is that aggregate with a loose bulk density of <1.20 g/cm^3 or a particle density not exceeding 2.00 g/cm^3 [3].

For several decades, LWA has been gradually gaining prominence over its higher density counterparts, a trend that is becoming more pronounced in recent years in response to the growing demand for lightweight concrete with thermal insulation capacity [4]. This suggests that the LWA industry will not only remain stable, but will grow in the coming years, so it is essential to understand the processes involved in their manufacturing in order to adapt them to the available raw materials.

From a physical point of view, a relatively recent study by Moreno-Maroto et al. [5] determined exactly the stages leading to the volumetric expansion process of LWA during firing. This work showed, among other aspects, that the gas required to form the porous structure of these materials is practically negligible, so that the achievement of a mineral matrix with a suitable viscosity is much more decisive. In addition, the role of organic carbon was given special relevance not as a gas generating agent for pore formation, but as a reducer of iron to form FeO, a flux inducing a suitable viscosity. These results broke with the classical belief that the emission of greater volumes of gas should correspond to greater bloating and that the role of organic carbon was primarily to release gases to increase porosity, a misconception that had been widespread since the early LWA research to the present day

* Corresponding author.
E-mail address: josemanuel.moreno@uam.es (J.M. Moreno-Maroto).

https://doi.org/10.1016/j.conbuildmat.2023.133152
Received 17 April 2023; Received in revised form 27 July 2023; Accepted 25 August 2023
Available online 4 September 2023

[6,7,8,9,10,11].

In this regard, a multitude of papers have been published on the role of the different primary components in the LWA formation process. All of them agree (correctly) that a basic source of alumninosilicates is essential, which will generally be the major component in the LWA formulation. It is common to use clays for this purpose, as they also present plastic characteristics to allow easy granulation / pelletization [4]. If the main component (e.g., clay) does not present self-expanding capacity when heated near its incipient melting point, it is necessary to incorporate additives of different nature to promote such effect. Most of the research in this regard, has focused on the study of iron, organic matter and fluxes as key elements. Some examples are shown below.

Moreno-Maroto et al. [12] studied the effect of an organic residue (olive pomace) when incorporated in percentages of 0, 1.25, 2.5, 5 and 10 wt% in three different clays, observing that the bloating effect is favored for low percentages of added organic matter (fundamentally close to 2.5 wt%), being inhibited for percentages $>$ 5 wt%. Recently, it has been demonstrated that the nature of the added organic component is much less relevant than the type of mineral matrix (e.g., the type of clay) in the bloating magnitude [13]. For their part, Bernhardt et al. [14] used a clay with 1 wt% of motor oil, testing the addition of Na_2CO_3 (2 and 5 wt%), SiO_2-silica fume (10 wt%), SiO_2-quartz (5 wt%), Fe_2O_3 (5 wt%) and Fe (5 wt%). The two iron phases studied acted positively on the formation of pores and bloating, while SiO_2, regardless of its species, had no effect in this regard. Na_2CO_3 was associated with lower bloating and a relevant decrease in viscosity at the surface level, giving rise to irregularly shaped LWAs that tended to stick together during heating in the kiln. Such results agree somewhat with those of Ren et al. [15], who observed a large external vitrification in fly ash-clay based LWAs when 10 wt% of sodium carbonate was added. Chien et al. [16] prepared five mixtures with different proportions of marine clay and a residue rich in iron and copper to which 1.5 wt% NaCl and Na_2CO_3 were added. The bloating was favored with the incorporation of these salts, especially with the latter.

Toyama and Kawamura [17] studied the kinetics of reactions leading to the formation of lightweight aggregates from a mixture comprised by fly ash and pulp waste liquor (final iron oxide content of 4.43 wt%). According to the findings of this work, the expansion would occur once the specimen is “sealed” to the outside atmosphere due to sintering. Likewise, this investigation suggested that the pores involved in the expansion are not those initially formed between the different constituents, but are formed secondarily during heating and that the firing conditions changed from oxidizing to reducing from the shell to the core [17]. In this sense, it was essential the role played by the reduction of iron in the core, which not only favored the development of adequate viscosity, but also the release of oxygen to form the LWA pores [17]. Sandrolini and Palmonari [18] prepared mixtures of kaolinitic clay with 5 and 10 wt% $CaCO_3$, as well as with 6 wt% Fe_2O_3, concluding that iron favors the expansion process in ceramic bodies, both by acting as a flux (thus generating viscous molten phases) and by the gases generated by its dissociation at high temperatures. Wie et al. [19] used an “acid clay” as the main component in seven mixtures varying the addition of Fe_2O_3 and activated carbon in a range between 0 and 15 wt% and 0–3 wt%, respectively. The bloating process was particularly satisfactory for those blends with carbon content equal to or higher than 2 wt% and Fe_2O_3 content above 5 wt%, due to iron reduction processes in the LWA core.

However, there are authors who have shown discrepancies with respect to the findings cited above. Thus, Wei et al. [20] studied a formulation with the following composition to develop lightweight aggregates: 69.82 wt% SiO_2, 14.92 wt% Al_2O_3, 6.37 wt% Fe_2O_3, 4.59 wt% K_2CO_3, 2.74 wt% Na_2CO_3 and 1.52 wt% $CaCO_3$. This mixture was pelletized and fired at different temperatures between 1000 and 1260 °C. Subsequent characterization studies showed that the iron retained mostly its Fe^{3+} oxidation state in the form of hematite, with hardly any amount of O_2 being released to form the pores. This outcome led Wei et al. [20] to conclude (misguidedly) that the LWA pore formation process based on iron reduction reactions was erroneous. In a previous study using a reservoir sediment, Wei and Lin [21] reached a similar conclusion, after producing artificial aggregates at 1050 °C and 1150 °C, because the iron contained in the starting sample (approx. 60% in the form of Fe^{2+}), tended to oxidize to Fe^{3+} in all cases, except in the core of those specimens fired at the highest temperature [21]. Such findings should have made these authors think that the choice of the correct firing temperature is also an essential factor in the manufacture of LWAs.

However, to date, the mechanism leading to LWA formation has not been consistently understood. This is due to the complexity of the potential interactions/synergies of the various components and the lack of a comprehensive and statistically consistent testing program. Four fundamental limitations are shown below, at least one of which is present in all the papers published to date on LWAs:

The number of mixtures covered is relatively small, which in turn may have two associated drawbacks. On the one hand, by studying a relatively narrow range of percentages, higher or lower proportions in which phenomena of interest may occur are neglected. On the other hand, if a wide range of percentages with few mixtures is intended to cover, precision is lost and uncertainty is gained again, but in this case in the range delimited between each pair of percentages.

The starting components are not pure in many cases, which makes it difficult to later interpret the results. For example, if the aim is to know how the addition of a certain type of iron oxide affects the LWA bloating process, but the starting clay already has iron in its composition (without knowing its oxidation state), control is lost on said variable. Therefore, it will not be possible to discern whether the observed behavior would be the same if the clay did not contain iron.

Only one variable is studied (for example, the effect of a carbonaceous residue on LWA bloating), without the possibility of studying other interactions with other critical factors.

A classical approach is used in planning the tests and interpreting the subsequent results. Thus, the analysis of such results is basically carried out *variable by variable* and *component by component*, without being able to know exactly their interactions and synergies.

Consequently, this work aims to effectively study the formation process of lightweight aggregates by overcoming the aforementioned drawbacks. For this purpose, four essential components of high purity will be employed: 1) clay, in this case a non-expansive kaolin, which is practically free of iron and fluxes; 2) organic carbon that acts as a reducing agent, in this case in the form of cork powder; 3) Na_2CO_3 as flux; and 4) powdered Fe_3O_4 as a source of iron, being one of the most interesting ingredients due to the role it may play in volumetric expansion.

It is important to note that this work is part of a broader investigation, in which the main objective is to understand how iron speciation interacts with the other aforementioned phases when obtaining ceramic materials, such as LWA. Thus, a recently published article by Moreno-Maroto et al. [22] using FeS_2 as iron source shows that pyrite does not favor any LWA bloating process when combined with kaolin, cork powder and Na_2CO_3, but rather the opposite, being therefore not suitable for producing LWAs. It is therefore necessary to clarify whether this behavior will be common to Fe_3O_4, or, as will be shown in this article, the findings will be totally different. For this purpose, the use of the pure phases mentioned above in combination with the application of statistical methods of *Mixture Experiments - Design of Experiments* (ME-DOE) will allow the effective study of the different interactions between the components, how they affect the technological properties and what would be the optimal formulations depending on each variable studied [22].

2. Materials and methods

2.1. Raw materials and their characterization

The present study focused on the use of four raw materials. Low-iron white kaolin (K) was the major component of the mixtures, coming from the quarry operated by the company Caobar, S.A. in Taracena (Guadalajara, central Spain). As it was previously ground and dried in the plant, it could be used directly. Its particle size distribution was determined by laser diffraction with a Coulter® LSTM 230 device. The carbon content was also determined, differentiating between total (TC), organic (OC) and inorganic (IC) carbon using a Shimadzu® TOC-V_{CSH} equipment. In turn, a Thermo ARL ADVANT'XP Sequential XRF was used to determine the chemical composition by X-Ray Fluorescence, correcting the loss-on-ignition (LOI) after calcining the kaolin at 1050 ℃ for 2 h in a muffle. The mineralogy of the sample was characterized by X-Ray Diffraction in both polycrystalline powder and oriented aggregates using a PANalytical® X'Pert Pro MRD diffractometer.

Another component studied was sodium carbonate anhydrous (Na_2CO_3, PanReac, for analysis, ACS), as a flux, referred to here with the abbreviation N. On the other hand, cork powder (C) (Eurotapón Núnez S.L., San Vicente de Alcántara, Spain) with particle size < 500 μm, calorific value of $\sim 3 \times 10^4$ kJ/kg and LOI of 100% [13] was used as an organic additive. Regarding the metallic additive, Fe_3O_4 powder (Alfa Aesar, 97% metal basis) with particle size below 325 μm in the form of magnetite (M) was used.

The thermal behavior of the samples was tested by simultaneous Differential Thermal Analysis-Thermogravimetric Analysis (DTA-TG), using a SETARAM® equipment, testing the samples in air and Ar atmosphere. The operating conditions were: maximum temperature: 1200 °C; ramp: 10 °C/min; air flow rate: 30 ml/min; Ar flow rate: 40 ml/min.

2.2. Planning, LWA manufacturing, characterization and validation

The protocol concerning the configuration of the formulations and the subsequent data analysis of the results obtained was carried out based on a *Mixture Experiments – Design of Experiments* (ME-DOE) approach using the statistical software R. The experimental sequence followed is shown in Fig. 1, which consists of 5 fundamental stages [22]: 1) Mixture planning; 2) LWA manufacturing; 3) LWA characterization; 4) Statistical analysis of results; and 5) Validation.

2.2.1. Mixture planning

ME-DOE uses regression models to determine the effect of the components of a mixture on the properties of the LWA. Usually, it is necessary to use more complex models than the linear model (quadratic, special cubic or cubic). Depending on the model considered a minimum number of samples is required to estimate the model coefficients.

The proposed ME-DOE has 4 components (K, C, N and M), with certain constraints considered, and is therefore a constrained mixture experiment [23]. In the case of the cork powder, C, the upper limit has been set at 5 wt% based on previous published results suggesting that higher percentages of organic matter may restrict the expansive process in LWAs [12,13]. Regarding N, the maximum value has also not exceeded 5 wt%, since preliminary tests have shown that higher amounts of sodium carbonate could hinder the firing of the pellets due to a high fluxing effect [22]. With regard to the iron phase, M, the maximum amount to be added has been set at 50 wt%, also based on previous tentative tests.

Using the *Xvert* function of the *mixexp* package of R [22,24], the necessary formulations have been defined to allow the estimation of a cubic model for each LWA property of interest. These have consisted of a total of 36 mixtures (Table 1). In accordance with the authors' previous study [22], the mixtures M1 to M10 do not contain any iron phase, so that these mixtures serve as the blank to know the effect of Fe_3O_4. In the case of kaolin, K, its proportion is determined by the proportion of the other components in the mixture, so that its value can range from a maximum of 100 wt% (mixture M1 in Table 1), to a minimum of 40 wt% (mixture M36 in Table 1). Considering the upper limit for each additive, the ME-DOE determines that 5 possible proportions have to be experimentally considered for each of them: 0, 12.5, 25, 37.5 and 50 wt% for M and 0, 1.25, 2.50, 3.75 and 5 wt% for C and N.

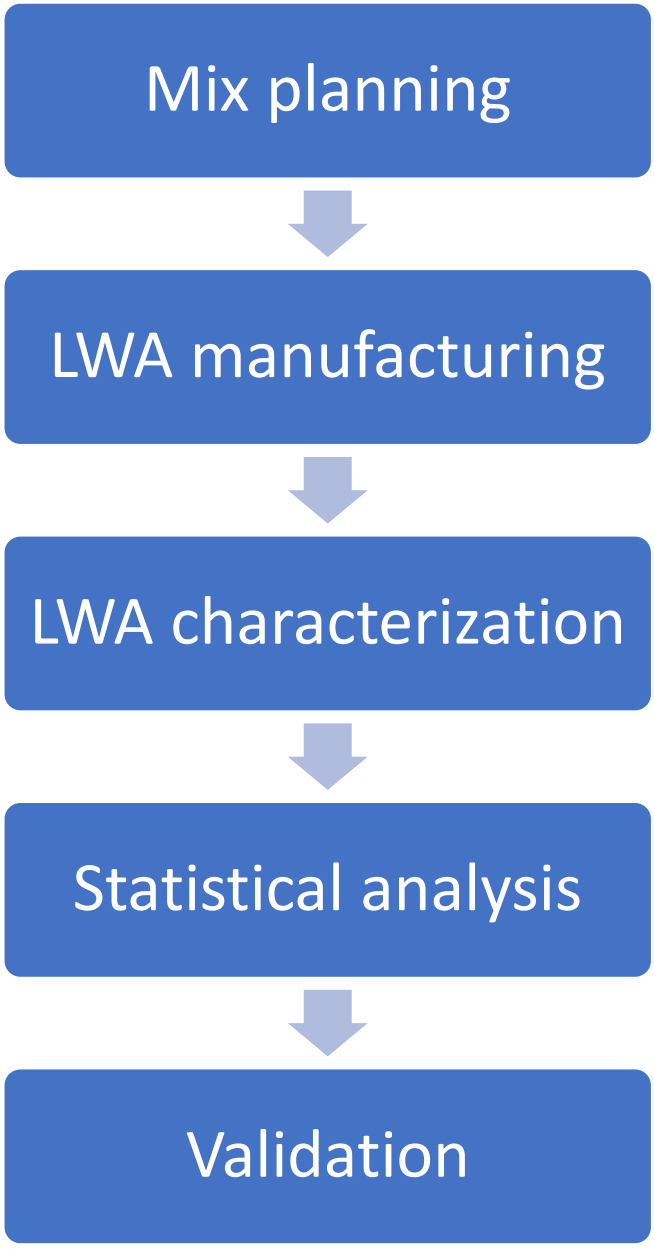

Fig. 1. Experimental sequence followed in this investigation based on the Design of Experiments – Mixture Experiments approach.

2.2.2. LWA manufacturing

Once the formulations in Table 1 were designed, first all the components were weighed and mixed homogeneously. A portion of the mixture was used to determine the Atterberg limits on plasticity, specifically the liquid limit (LL) by the Casagrande cup method [25] and the plastic limit (PL) by the Moreno-Maroto and Alonso-Azcárate [26] bending method, determining the plasticity index (PI) as the difference between both parameters. Based on the observed workability, the PL value was used to calculate the optimum moisture content (W_{OP}) as W_{OP}

Table 1
Composition and plasticity of the starting mixtures studied. K = kaolin; M = magnetite (Fe_3O_4); C = cork powder (organic matter); N = sodium carbonate (Na_2CO_3).

Components (%)					Plasticity				
Mix.	K	M	C	N	LL	PL	PI	PI/LL	W_{OP} (%)
M1[a]	100	0	0	0	42.1	22.7	19.5	0.46	33.9
M2[a]	97.5	0	2.5	0	45.1	24.2	20.9	0.46	36.2
M3[a]	97.5	0	0	2.5	42.5	22.4	20.1	0.47	33.5
M4[a]	95	0	5	0	48.1	25.7	22.3	0.46	38.5
M5[a]	95	0	0	5	42.9	22.1	20.8	0.48	33.1
M6[a]	95	0	2.5	2.5	45.5	23.9	21.6	0.47	35.8
M7[a]	95	0	2.5	2.5	45.5	23.9	21.6	0.47	35.8
M8[a]	92.5	0	5	2.5	48.5	25.5	23.0	0.47	38.0
M9[a]	92.5	0	2.5	5	45.9	23.6	22.2	0.48	35.3
M10[a]	90	0	5	5	48.9	25.2	23.7	0.48	37.6
M11	85	12.5	1.25	1.25	45.0	24.1	20.9	0.47	36.0
M12	82.5	12.5	3.75	1.25	48.4	25.8	22.6	0.47	38.6
M13	82.5	12.5	1.25	3.75	45.4	23.7	21.7	0.48	35.5
M14	80	12.5	3.75	3.75	48.9	25.5	23.4	0.48	38.1
M15	75	25	0	0	42.9	23.2	19.7	0.46	34.6
M16	72.5	25	2.5	0	46.8	25.2	21.6	0.46	37.7
M17	72.5	25	0	2.5	43.4	22.8	20.6	0.47	34.1
M18	70	25	0	5	43.9	22.4	21.5	0.49	33.6
M19	70	25	5	0	50.8	27.3	23.5	0.46	40.8
M20	67.5	25	5	2.5	51.3	26.9	24.5	0.48	40.2
M21	67.5	25	2.5	5	47.9	24.5	23.4	0.49	36.6
M22	65	25	5	5	51.9	26.5	25.4	0.49	39.6
M23	60	37.5	1.25	1.25	44.2	23.2	21.0	0.48	34.6
M24	57.5	37.5	1.25	3.75	44.8	22.7	22.1	0.49	34.0
M25	57.5	37.5	3.75	1.25	49.0	25.6	23.3	0.48	38.3
M26	55	37.5	3.75	3.75	49.6	25.2	24.5	0.49	37.6
M27	50	50	0	0	39.0	20.3	18.7	0.48	30.3
M28	47.5	50	2.5	0	44.9	23.4	21.6	0.48	34.9
M29	47.5	50	0	2.5	39.8	19.8	20.0	0.50	29.5
M30	45	50	2.5	2.5	45.7	22.8	22.9	0.50	34.1
M31	45	50	2.5	2.5	45.7	22.8	22.9	0.50	34.1
M32	45	50	5	0	50.9	26.4	24.4	0.48	39.5
M33	45	50	0	5	40.6	19.2	21.3	0.53	28.7
M34	42.5	50	2.5	5	46.6	22.2	24.3	0.52	33.3
M35	42.5	50	5	2.5	51.7	25.9	25.9	0.50	38.6
M36	40	50	5	5	52.6	25.3	27.3	0.52	37.8

[a] Mixtures M1 to M10 are used as a reference for the study of Fe_3O_4 effect. Their results are also published in the work of Moreno-Maroto et al. [22], in which FeS_2 was studied instead of Fe_3O_4.

= 1.495 × PL [26].

The amount of distilled water corresponding to W_{OP} was added to each formulation, intimately kneading with a metal spatula until a homogeneous workable dough was obtained. After a maceration period of 24 h in hermetic conditions, the wet material was extruded in the form of a 6-mm-diameter cord through a Nannetti® pneumatic extruder, to be then cut every 15 mm, so that the 6 × 15 mm cylinders obtained were rounded by hand until obtaining spherical granules of around 9.3 mm in diameter. These granules were dried, first at room temperature and subsequently in an oven at 105 °C until constant weight (48 h of drying was enough). It is important to note that although the granulation process has been carried out manually in this research (laboratory scale work), there are mechanized systems for this purpose at the industrial level (extruders, granulators, etc.). Therefore, there would be no impediment to scaling up the process in this sense.

The dry granules were fired in batches of 25 specimens in a Nannetti® TOR-R 120–14 tubular kiln whose rotation speed was set at 2.5 r.p.m. In agreement with the firing times normally employed at industrial level for the production of LWAs, which are in the order of minutes [4], the total firing time was 12 min. While the first 2 min were applied as preheating in the first section of the tube to avoid premature bursting of the specimens, the firing itself for the remaining 10 min took place in the middle. During firing, the material was subjected to the maximum possible temperature, in order to favor the greatest degree of expansion and sintering. Just above this temperature, the firing process would not be viable since the granules would begin to adhere to each other and to the kiln walls. This temperature was established for each mixture through preliminary trials based on trial and error. As will be seen in the following sections, this temperature will depend largely on the composition of the mixture. The sintered aggregates were left to cool at room temperature until characterization.

2.2.3. LWA characterization

The LOI during the preheating (LOI_{preh}) and complete firing (LOI_{firing}) stages was determined in 25 specimens as the percentage change in weight before and after heating in the rotary kiln. Similarly, the bloating index (*BI*) was calculated as the percentage change in size experienced by those same pellets during the complete firing [27]. The following parameters related to density were experimentally determined: loose bulk density (ρ_b; [28]), apparent density (ρ_a; [29]) and oven-dry density (ρ_{rd}; [29]). The relative density of the aggregate solid phase (ρ_{solid}) was estimated according to Eq. (1) as follows:

$$\rho_{solid} = 2.6 \times [K/(K+M)] + 5 \times [M/(K+M)] \quad (1)$$

where:

K and M represent respectively the percentages of kaolin and magnetite used; 2.6 (g/cm^3) is the ρ_{solid} of a conventional lightweight expanded clay aggregate [30,31]; 5 (g/cm^3) is the approximate density of magnetite, as well as of Fe_2O_3, which could be formed by their oxidation. In the case of the organic component and Na_2CO_3, it can be considered that they would not significantly affect this parameter, because their proportion in the mixtures is low and they tend to decompose during heating.

Once the ρ_a, ρ_{rd} and ρ_{solid} values were known, the total (P_T), open (P_O) and closed porosity (P_C) values were computed according to De Santiago Buey and Raya García [32] and Bernhardt et al. [33]. A new

parameter developed in this study, called *Open porosity volume per specimen* (V_{PO}, in mm^3), has been calculated according to the following equation:

$$V_{PO} = 4/3[\pi(\theta/2)^3] \times (P_O/100) \quad (2)$$

where:

the first part of the equation refers to the total volume of an individual aggregate specimen (mm^3), where Ø is the diameter shown in Table 3. The second part is the multiplying factor depending on the open porosity, P_O.

Water absorption during 24 h (WA_{24}) was determined simultaneously with the density tests, following the EN-1097–6 [29] standard. Mechanical strength was measured according to Yashima et al. [34] and Li et al. [35] on 25 specimens of each variety through a crushing test conducted on single aggregates (S) using a Nannetti®FM 96 press.

Using the same XRD equipment indicated in Section 2.1, the mineralogy of one selected aggregate has been determined after grinding < 63 μm. In this case, the interpretation has been carried out by Rietveld refinement in order to quantify both crystalline and amorphous phases following the protocol developed by Moreno-Maroto et al. [36].

2.2.4. Statistical analysis of results

As can be seen in Fig. 1, the fourth step carried out was to statistically analyze the results obtained for the LWA characterization stage. For this purpose, four technological variables (BI, ρ_{rd}, WA_{24} and S) were selected, relating to the compositional characteristics of the mixtures using the software R [22]. Different regression models (cubic, special cubic, quadratic and linear) have been estimated for the obtained measurements and after a comparison between them, the most appropriate one has been selected. Analysis of diagnostic plots (Residuals vs Fitted, Q − Q plots on normality, Scale − Location and Residuals vs Leverage) and ANOVA has supported this [22].

The next step consisted of applying the models to obtain effect plots, as well as response surface plots (contour plots) to see how the response, i.e. the property under analysis, changes for different values of the mixture components. Finally, the optimum values of the mixtures have been calculated to maximize or minimize the different responses of the four technological properties studied [22]. In the cases of BI, WA_{24} and S, the optimum has been considered as the maximum value of the function, while the minimum was considered for ρ_{rd}.

2.2.5. Validation

The last step was the validation of the statistically obtained models (Fig. 1). For this purpose, aggregates have been manufactured from the mixtures corresponding to the optimum values of each property, comparing the results obtained experimentally for the temperature and technological properties studied, with respect to those estimated through the statistical models [22].

3. Results and discussion

3.1. Characteristics of the kaolin and the raw mixtures

The compositional characteristics of the kaolin are shown in Table 2. K is a white kaolin that does not contain carbon, so the only contribution of this element to the mixtures would come from the cork powder added, where applicable. The inorganic nature of K is reflected in its mineralogical composition, in which there is a predominance of kaolinite, with quartz and illite appearing as minor phases. In the case of the chemical composition, the high proportions of SiO_2 (51%) and Al_2O_3 (35%) are noteworthy, which contrasts with the low percentages of other elements, including those considered as fluxes, among which are iron oxides and those of alkaline and alkaline earth metals. Focusing on iron, its content in this kaolin is very low (only 0.4%). According to Moreno-Maroto et al. [22], this is positive, since in order to control the effect of the Fe_3O_4 phase in the mixtures, it was considered essential that the kaolin contained as little iron as possible.

Regarding the particle size distribution, Fig. 2 reveals that K is a very fine-grained clay, with an average particle size of 8.3 μm, 90% of particles smaller than 18.2 μm (see d90) and 50% of particles smaller than 4.6 μm (see d50). The differential particle size distribution presents five modes located at about 111, 33, 10, 4.7 and 0.4 μm, the last two being the most marked (mainly the peak around 4.7 μm).

This predominantly fine particle size, together with the phyllosilicate-rich mineralogy have resulted in LL, PL and PI values of 42.1, 22.7 and 19.5, respectively (see M1 formulation in Table 1). The incorporation of the different additives has led to changes in these values, whose ranges have been 52.6–39 for LL, 27.3–19.2 for PL and 27.3–18.7 for PI, which has translated into W_{OP} values between 28.7% and 40.8% (Table 1). Despite these variations, the workability and toughness of the material have hardly been affected, as shown by the fact that the PI/LL ratio remains in all cases close to 0.5 in agreement with the previous study using pyrite [22], values typical of clayey materials with adequate plasticity for extrusion and pelletizing [37].

3.2. Technological characteristics of the aggregates obtained before modeling

The 36 types of aggregate obtained for modeling are shown in Fig. 3. It is noticeable how those varieties that do not contain iron are completely white and do not present a differentiation between shell and core (M1 to M10). However, the incorporation of magnetite has led to the formation of the typical LWA shell-core structure in almost all the aggregates, with the exception of some varieties (M13, M15, M17, M18 and M27), which are characterized by substantial shrinkage during sintering, as well as no or very low C content (Table 1). The shell of the aggregates containing M is reddish in color, and the core is generally grayish or black. These colors could be related to the oxidation of magnetite to Fe_2O_3 in the crust and its reduction to FeO in the core, processes that will be explained in more detail in section 3.3.1.

The main characteristics of the sintered aggregates are shown in Table 3. As for the distribution of the data, the skewness values are generally close to 0, which would indicate that the distribution is quite symmetrical for the properties studied. The kurtosis values are negative in all cases, which suggests a platykurtic (flattened) distribution, with a lower concentration of data around the mean. Analyzing the weight of the standard deviation with respect to the mean through the coefficient of variation (CV), it can be seen that the dispersion of the data differs depending on the variable studied. The results obtained for each parameter are discussed in detail below.

3.2.1. Firing temperature and loss on ignition

As shown in Table 3, the lowest CV is that of temperature (6%). The minimum temperature applied was that of mixtures M35 and M36 (1135 °C), 210 °C difference with respect to the maximum recorded (1345 °C) for mixtures M1, M2, M3 and M4, whose high kaolin content

Table 2
Main characteristics of the kaolin used in this investigation.

	Carbon content (%)				Chemical composition, oxides (%)										Mineralogy	
Clay name	TC	IC	OC	LOI (%)	SiO_2	Al_2O_3	Fe_2O_3[a]	Na_2O[a]	K_2O[a]	MgO[a]	CaO[a]	TiO_2	SO_3	P_2O_5	Major	Minor
Kaolin	0.0	0.0	0.0	12.6	50.9	35.0	0.4	0.0	0.4	0.1	0.1	0.1	0.4	0.1	Kaolinite	Quartz, Illite

[a] Fluxing oxide.

Table 3
Main characteristics of the aggregates obtained from the starting formulations.

Mixture	T (°C)	Ø (mm)	*BI* (%)	$LOI_{rotary\ kiln}$ (%)		Density (g/cm^3)				WA_{24} (%)	Porosity, *P* (%)			*S* (MPa)
				LOI_{preh}	LOI_{firing}	ρ_b	ρ_a	ρ_{rd}	ρ_{solid}[b]		P_T	P_O	P_C	
M1[a]	1345	8.3	−9.1	11.3	12.8	1.10	2.58	1.94	2.60	12.6	25.3	24.6	0.6	9.7
M2[a]	1345	8.4	−8.3	14.1	14.9	0.98	2.33	1.75	2.60	14.3	32.8	25.0	7.9	7.3
M3[a]	1345	8.2	−11.3	11.3	12.9	1.22	2.50	2.14	2.60	6.7	17.6	14.3	3.4	18.1
M4[a]	1345	8.7	−7.9	15.6	17.2	0.88	2.12	1.52	2.60	18.5	41.4	28.2	13.2	5.5
M5[a]	1260	8.7	−7.1	12.2	14.9	0.98	2.43	1.75	2.60	16.1	32.9	28.2	4.7	7.9
M6[a]	1330	8.2	−11.3	14.9	15.9	1.06	2.25	1.88	2.60	8.8	27.7	16.5	11.2	12.3
M7[a]	1330	8.3	−10.3	15.1	16.0	1.08	2.26	1.91	2.60	8.1	26.5	15.6	10.9	12.5
M8[a]	1330	8.2	−12.4	16.0	17.6	0.99	2.08	1.75	2.60	9.2	32.8	16.2	16.6	9.6
M9[a]	1250	8.7	−7.2	14.4	16.6	0.88	2.21	1.58	2.60	18.0	39.3	28.5	10.9	5.0
M10[a]	1230	8.7	−7.9	17.5	18.4	0.83	2.14	1.47	2.60	21.4	43.6	31.6	12.0	3.8
M11	1320	8.3	−9.4	11.4	12.8	1.16	2.21	2.03	2.91	4.1	30.1	8.3	21.9	5.6
M12	1275	9.0	−3.0	13.6	15.0	0.78	1.60	1.39	2.92	9.3	52.3	13.0	39.3	5.4
M13	1215	8.5	−6.4	12.4	13.4	1.00	2.27	1.75	2.92	13.1	40.0	23.0	17.1	6.2
M14	1195	9.1	−2.3	13.9	15.8	0.77	1.57	1.36	2.92	9.6	53.4	13.1	40.3	7.5
M15	1335	8.0	−14.0	9.3	10.1	1.44	2.76	2.47	3.20	4.2	22.8	10.5	12.4	13.3
M16	1335	12.2	33.3	10.9	12.3	0.40	0.83	0.75	3.22	12.7	76.8	9.5	67.2	0.9
M17	1340	7.8	−15.5	9.8	10.6	1.50	2.61	2.59	3.22	0.3	19.3	0.8	18.5	19.4
M18	1199	8.5	−6.7	10.7	11.0	1.15	2.67	2.07	3.23	10.9	36.1	22.6	13.4	5.6
M19	1220	11.8	30.1	12.3	16.7	0.32	0.67	0.61	3.23	14.6	81.1	8.9	72.2	0.3
M20	1160	11.6	24.1	13.6	15.7	0.33	0.72	0.63	3.25	20.9	80.7	13.1	67.6	0.8
M21	1170	11.3	21.7	13.0	14.5	0.39	0.85	0.74	3.25	16.3	77.1	12.2	64.9	1.9
M22	1140	11.9	29.4	13.9	16.2	0.30	0.65	0.58	3.27	19.2	82.4	11.1	71.3	1.1
M23	1315	10.5	13.8	9.5	10.0	0.62	1.31	1.16	3.52	9.7	67.1	11.3	55.8	2.2
M24	1230	9.3	1.7	9.5	10.8	0.85	1.79	1.59	3.55	7.0	55.1	11.2	43.9	4.3
M25	1215	14.1	52.6	10.9	14.5	0.19	0.39	0.36	3.55	22.0	89.9	7.9	81.9	0.1
M26	1185	12.8	36.9	10.9	14.1	0.28	0.56	0.51	3.57	14.4	85.6	7.4	78.2	0.3
M27	1345	8.2	−12.0	5.9	6.9	1.56	2.85	2.65	3.80	2.7	30.3	7.1	23.2	13.6
M28	1265	12.1	29.7	7.3	10.5	0.40	0.77	0.72	3.83	9.5	81.2	6.9	74.3	0.4
M29	1305	8.4	−10.5	6.3	7.3	1.41	2.60	2.45	3.83	2.4	36.1	5.9	30.2	14.9
M30	1245	11.8	25.7	8.6	11.3	0.42	0.87	0.82	3.86	7.2	78.8	5.9	73.0	0.6
M31	1245	11.6	25.0	8.6	11.6	0.43	0.84	0.79	3.86	8.0	79.5	6.4	73.2	0.6
M32	1145	12.1	30.2	8.4	13.5	0.34	0.81	0.72	3.86	16.0	81.4	11.5	69.9	0.3
M33	1235	8.2	−14.1	5.5	9.0	1.61	2.97	2.87	3.86	1.1	25.6	3.3	22.4	18.1
M34	1225	10.3	9.5	10.5	12.0	0.67	1.31	1.23	3.90	5.0	68.4	6.2	62.2	1.5
M35	1135	9.3	0.8	9.4	14.7	0.73	1.43	1.36	3.90	3.3	65.0	4.6	60.4	1.4
M36	1135	9.0	−2.9	9.7	14.9	0.86	1.66	1.57	3.93	3.5	60.1	5.6	54.6	1.3
Max	1345	14.1	52.6	17.5	18.4	1.61	2.97	2.87	3.93	22.0	89.9	31.6	81.9	19.4
Min	1135	7.8	−15.5	5.5	6.9	0.19	0.39	0.36	2.60	0.3	17.6	0.8	0.6	0.1
Mean	1257	9.7	4.9	11.3	13.4	0.83	1.74	1.48	3.23	10.6	52.1	13.2	38.9	6.1
St. Dev.	71.2	1.7	18.9	2.9	2.9	0.40	0.79	0.68	0.50	6.1	23.4	8.1	27.3	5.8
CV (%)	6	18	389	26	21	48	46	46	16	58	45	61	70	95
Kurtosis	−1.3	−0.6	−0.6	−0.5	−0.4	−0.9	−1.4	−0.9	−1.5	−0.9	−1.6	−0.3	−1.7	−0.3
Skewness	−0.2	0.8	0.8	0.0	−0.4	0.2	−0.2	0.2	0.0	0.2	0.2	0.8	0.2	0.9

[a] Mixtures M1 to M10 are used as a reference for the study of Fe_3O_4 effect. Their results are also published in the work of Moreno-Maroto et al. [22], in which FeS_2 was studied instead of Fe_3O_4.
[b] Estimated value according to Eq. (1).

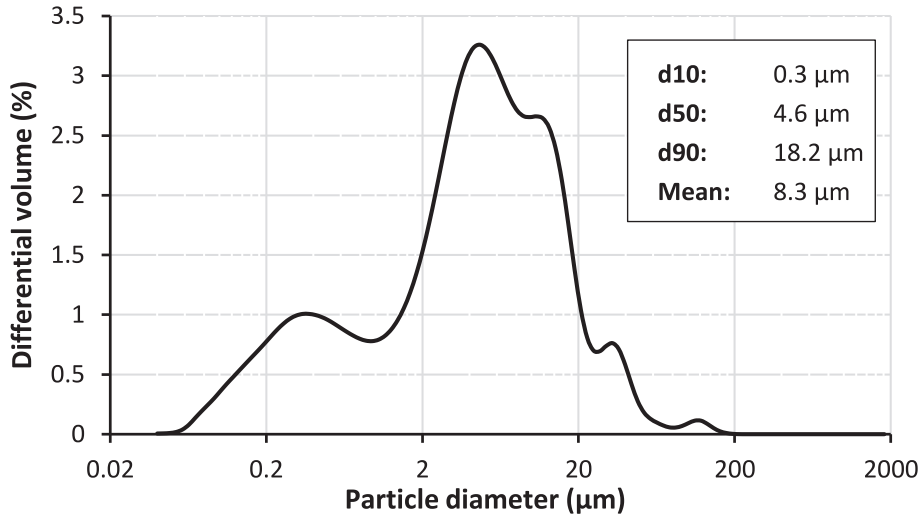

Fig. 2. Particle size distribution of the kaolin used in this research [22].

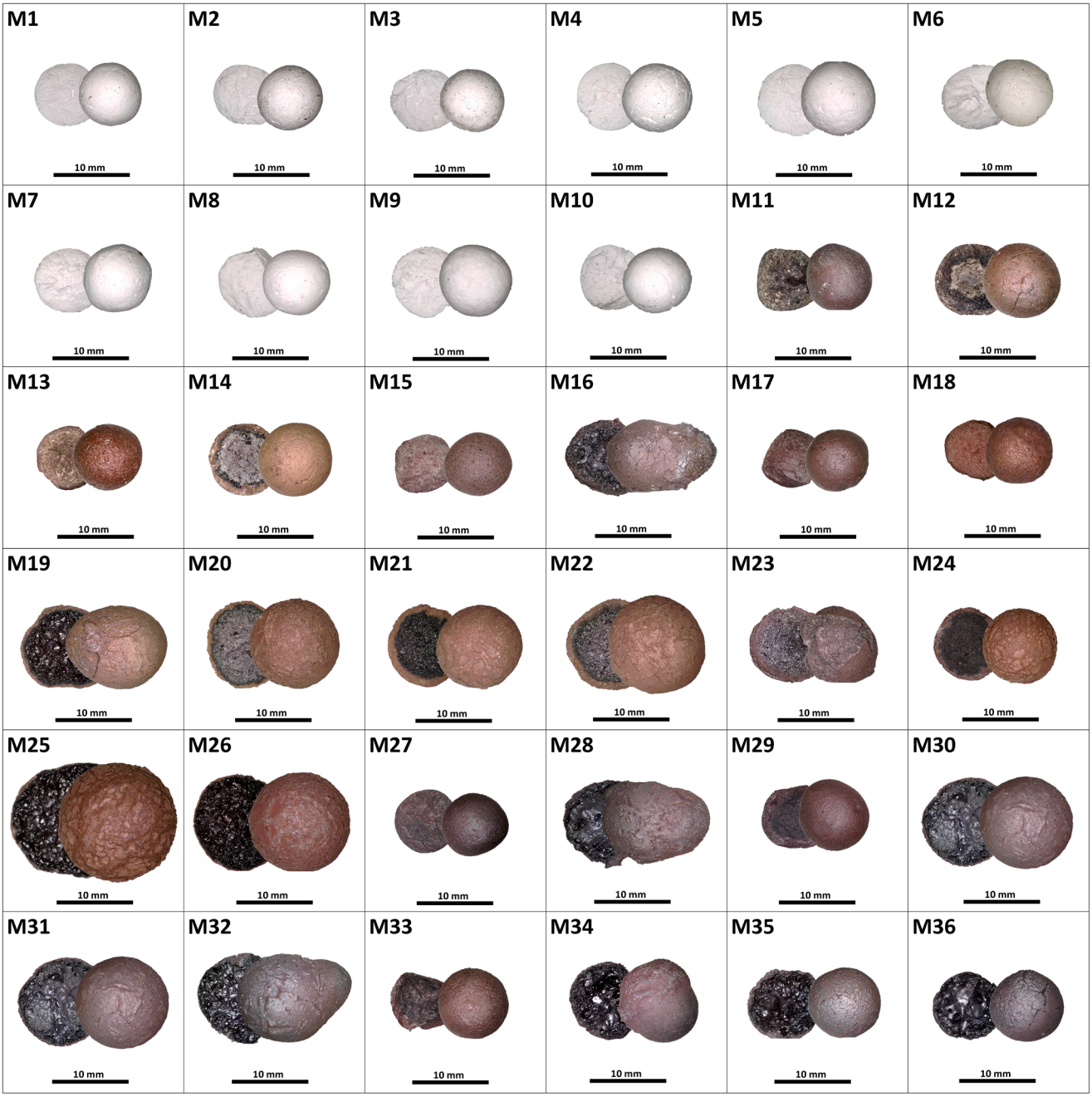

Fig. 3. Outer face (shell) and core of the 36 varieties of aggregate initially obtained to prepare the statistical models. M1 to M10 serve as a reference (without iron) [22].

demonstrates the refractory character of this clay [22]. According to Table 1, the former present 50 wt% Fe_3O_4 added, while the latter have no magnetite at all, so that, regardless of the role that the addition of C and N may have played, the incorporation of magnetite in the mixtures seems to favor the lowering of the working temperature. This could be positive if the aim is to reduce the energy consumption associated with heating during manufacture, with a consequent reduction in environmental impact.

In the case of the LOI recorded during both preheating and complete firing, it can be seen that the dispersion of the data is relatively low (CV of 26 and 21%, respectively) if compared with most of the properties measured. In general terms, it is observed that the greatest gas loss occurs during preheating, which is in agreement with previous studies [5]. The mixtures with the lowest LOI values are M27, M29 and M33 (<9%), whose main characteristics are the high content of Fe_3O_4 (50%), the relatively low proportion of kaolin (45–50%) and the absence of organic agent. The rest of the samples present LOI values above 10%, the maximum values being found in samples M4, M8 and M10 (16–18%), which are characterized by high proportions of K (90–95%) and C (5%). In agreement with the DTA-TG curves in Fig. 4 and the findings of the previous study [22], such results indicate that the main sources of gas are the organic additive (Fig. 4c: exothermic decomposition releasing H_2O(g), CO_2 and/or CO between 250 and 500 °C) and the kaolin itself (Fig. 4a: endothermic dehydroxylation between 450 and 600 °C releasing H_2O(g)). The decomposition of sodium carbonate also implies the formation of CO_2 (Fig. 4d: endothermic dehydroxylation above 850 °C). A tiny proportion of these gases will be retained in the mineral matrix, facilitating the process of formation of closed pores and the

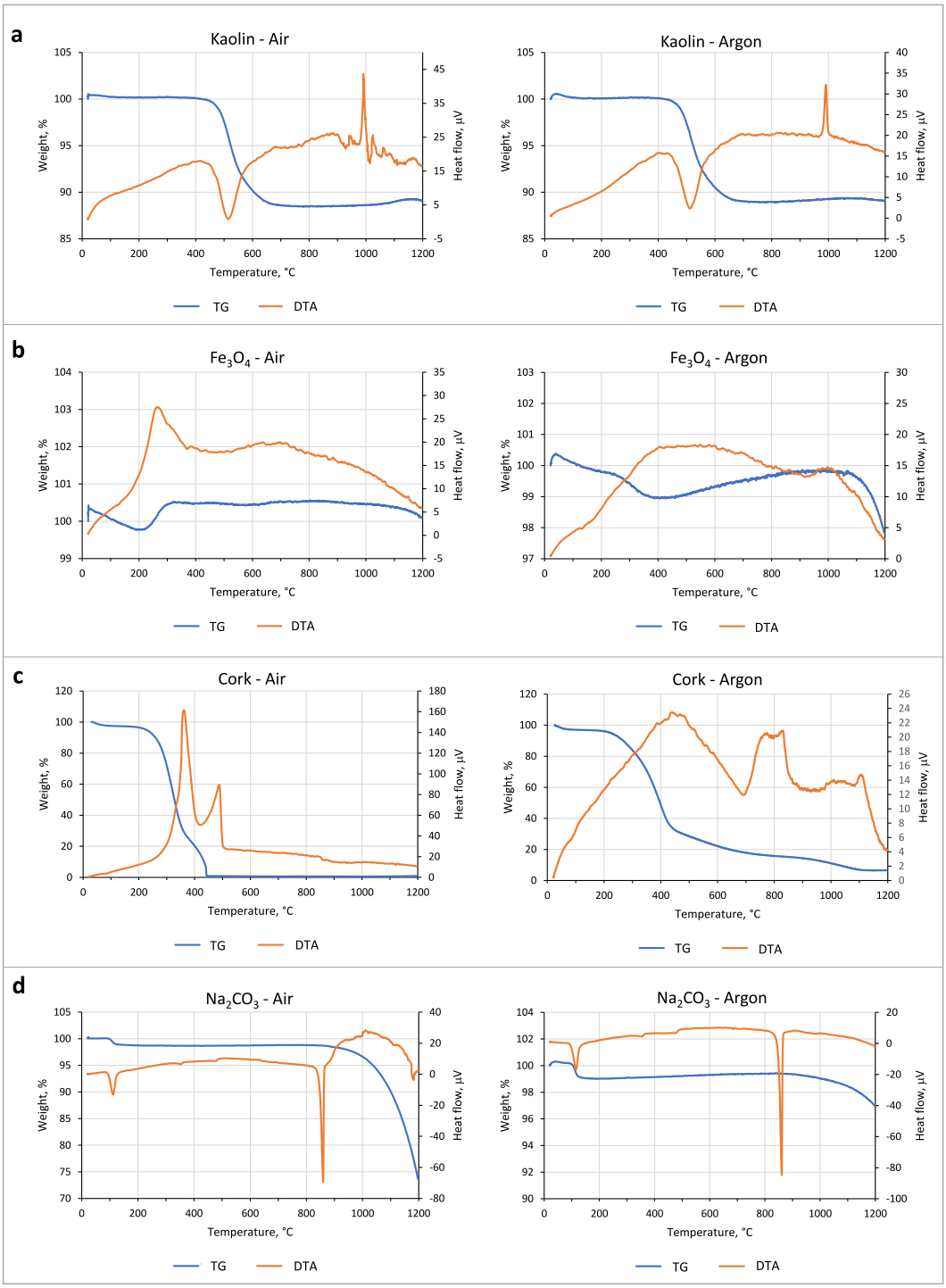

Fig. 4. DTA-TG graphs in air and Ar atmosphere for the primary components of the mixtures: (a) kaolin; (b) magnetite; (c) cork powder; (d) sodium carbonate.

concomitant expansion of those specimens of lower density [5].

3.2.2. *Density, bloating index and porosity*

Regarding aggregate density, out of the 36 formulations shown in Table 3, only seven (M3, M11, M15, M17, M27, M29 and M33) would not meet the requirements of $\rho_b < 1.20$ g/cm^3 or $\rho_{rd} < 2.00$ g/cm^3 established by the EN-13055–1 [3] standard for lightweight aggregates. As can be seen in Fig. 5a,b, there is a linear correlation between the three types of densities obtained experimentally, so, in order to avoid redundancy, the discussion will focus on the ρ_{rd} parameter. The highest ρ_{rd} value is that of formulation M33 (2.87 g/cm^3), followed by M27 (2.65 g/cm^3), M17 (2.59 g/cm^3) and M29 (2.45 g/cm^3), characterized by the addition of high magnetite proportions (whose density is about 5 g/cm^3), and the absence of organic residue, which seems to be important to obtain a lighter structure. In contrast, mixture M25 (K = 57.5% + M = 37.5% + C = 3.75% + N = 1%; Table 1) has the lowest density of all ($\rho_{rd} = 0.36$ g/cm^3) coinciding with the fact that this mixture is the one that has also expanded the most, which would be in line with the expected behavior, since there is an inverse relationship between density and bloating index (Fig. 5c). Thus, while the aggregate diameter data (Ø in Table 3) show a relatively low dispersion (CV = 18%), the *BI* results exhibit the highest CV of all (389%). Although the average *BI* of the

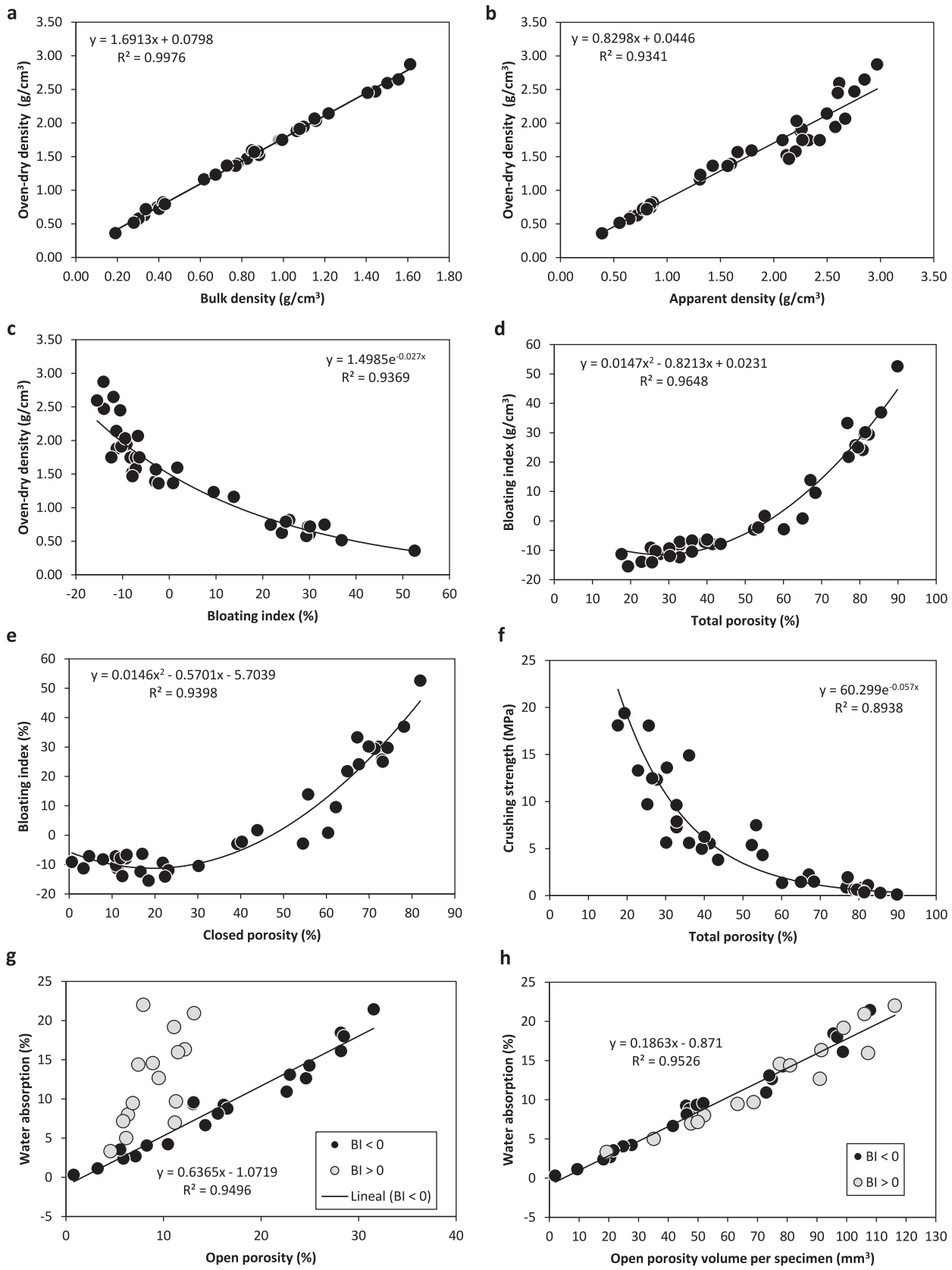

Fig. 5. Relationship between different key parameters in the Fe_3O_4 study: (a) ρ_b vs ρ_{rd}; (b) ρ_a vs ρ_{rd}; (c) *BI* vs ρ_{rd}; (d) P_T vs *BI*; (d) P_C vs *BI*; (d) P_T vs *S*; (e) P_O vs WA_{24}; (f) V_{PO} vs WA_{24}.

specimens obtained is 4.9%, the range varies between a minimum *BI* of −15.5% (M17) and a maximum of 52.6% (M25). It is noteworthy that kaolin alone is unable to expand (M1 in Table 3), so that positive effects in this regard would be attributable to the added components. Due to the complexity of the possible interactions between the components of the mixtures, the *BI* results have been analyzed based on statistical models that will be discussed in Section 3.3.

On the other hand, as expected, there is also a direct relationship between the increase in *BI* and total porosity (Fig. 5d), specifically of closed type (Fig. 5e). This is related to the formation of a viscous glassy matrix, which is capable of trapping even the negligible amounts of gas responsible for bloating [5,36]. Thus, P_T ranges from 17.6% (M3) to 89.9% (M25), P_O from 0.8% (M17) to 31.6% (M10) and P_C from 0.6% (M1) to 81.9% (M25), with CVs of 45, 61 and 70%, respectively, indicative of a wide variety of results among the different mixtures. It is important to note that the representation of the mixtures in the Riley [6] diagram does not follow a pattern that allows establishing a clear relationship between the chemical composition, the increase in expansion and the decrease in density (Fig. 6). In fact, the most expanded and lightest LWA formulation is far away from the theoretical bloating area. This agrees with the work published by Dondi et al. [11], which showed that the Riley triangle cannot be used predictively to determine the expansion potential of a mixture on the basis of its chemical composition.

3.2.3. Water absorption and crushing strength

In the case of water absorption, the variation between samples is also large (CV = 58%). M25 presents the highest WA_{24} value (22%), followed by M10 and M20 in the same order, while the minimum figure is that of the M17 mixture (0.3%). These results are within the range of values normally obtained according to the literature [5,12,22,36]. Water absorption in lightweight aggregates is mainly due to the presence of open and interconnected pores. However, as can be seen in Fig. 5g, the correlation between WA_{24} and P_O is only good in those formulations that have not expanded ($BI < 0$), so that some formulations with $BI > 0$ present high water absorption despite their relatively low P_O value, something that a priori may seem contradictory. However, it is important to understand that the P_O value is relative (%) with respect to the total volume of the aggregate, and therefore, in absolute terms, the volume occupied by these pores can be higher in expanded aggregates with respect to non-expanded aggregates, even though the former have a lower P_O. Thus, Fig. 5h illustrates that when P_O is transformed into V_{PO}, as expected, the correlation is now high in relation to WA_{24}, increasing with respect to each other.

On the other hand, the increase in porosity negatively affects the mechanical strength (Fig. 5f), so, according to Table 3, the range of *S* values is relatively wide, between 0.1 MPa (M25, the most expanded and porous aggregate) and 19.4 MPa (M17, the most shrunken one). Despite this, in general the samples show crushing strength results in the same order or higher than those of commercial lightweight aggregates, such as Argex AR 4/10–550, whose *S* value is 1.3 MPa [12].

Regarding the role of the additives, no simple conclusions can be drawn based on the results in Table 3, so the influence of each of the components both on *S* and WA_{24} (along with those of *BI* and ρ_{rd}) will be discussed in the next section after obtaining the best-fitting statistical model.

3.3. Statistical analysis and modeling

As shown in Fig. 1, once the aggregate characterization has been completed, the next step is to fit the best regression model for each of the selected properties (*BI*, ρ_{rd}, WA_{24} and *S*). The procedure was as follows: for each selected model, a diagnosis was carried out, and, in those cases where the model did not meet the requirements, it was modified to obtain a statistically adequate model (details are omitted for brevity). The coefficients of the models obtained are shown in Table 4. The model for each property considered is discussed below.

3.3.1. Bloating index modeling and the expansion mechanism in LWA

After the diagnosis, the estimated model for *BI* was not adequate. A Box-Cox transformation of the response variable was performed to find the most appropriate model, revealing that the best fit was a cubic model for $\log(BI + 20)$. Fig. 7a and Fig. 8a show the response surface and effect plots for *BI*, respectively. In the case of Fig. 7, since there are four compositional variables (K, C, N and M), three fixed values of K (50 wt%, 70 wt% or 90 wt%) have been selected, plotting the rest of the variables for each of these kaolin percentages. The feasible area (the one of interest for this work) is the rhombus delimited between the axis of C (organic matter), M (Fe_3O_4) and the dashed line that appears in each figure. This is also applicable to the rest of the properties under study,

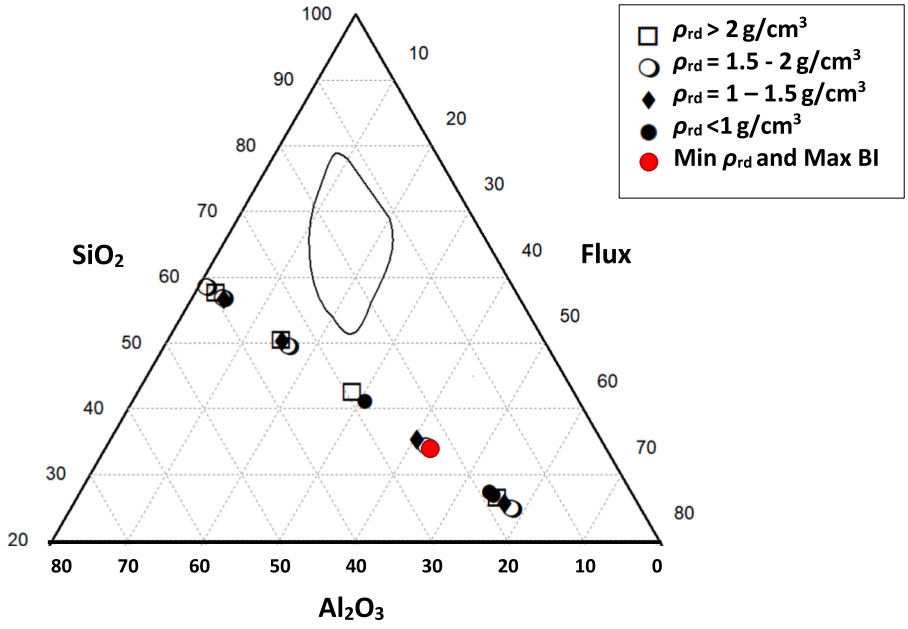

Fig. 6. Location of some representative formulations from the Fe_3O_4 on the Riley [6] diagram.

Table 4
Coefficients of the regression models (cubic) and analysis of variance obtained for each key property.

	BI [log (*BI* + 20)]	ρ_{rd}	WA_{24}	*S* [$\sqrt{S}$]
K	2.3	2.0	12.6	3.3
M	−9.4	12.9	−169.7	16.6
C	11832.3	−2871.6	21958.1	−53830.9
N	8409.9	−7553.8	173952.3	−26277.5
cubic (K,M)	−19.3	15.5	−265.2	15.1
cubic (K,C)	6561.6	−1605.5	11508.1	−26264.5
cubic (K,N)	4210.7	−3839.8	87436.3	−13109.5
cubic (M,C)	7972.1	−3088.0	15593.6	−31527.6
cubic (M,N)	4811.9	−4371.2	97902.6	−14836.6
cubic (C,N)	−1260.6	−1965.3	77914.7	5800.6
K:M	22.6	−19.5	325.3	−24.6
K:C	−18355.4	4460.2	−33374.0	82985.1
K:N	−12633.2	11403.9	−261699.7	39447.1
M:C	−19710.2	5834.1	−37351.1	84998.2
M:N	−13219.4	11918.0	−271706.8	41027.9
C:N	−27660.3	14303.3	−307177.1	124801.5
K:M:C	14892.7	−4925.5	28870.8	−60973.3
K:M:N	9109.3	−8273.4	186580.1	−27961.3
K:C:N	17719.3	−9087.0	211104.9	−87146.5
M:C:N	19781.7	−11097.0	221385.0	91349.2
F-test	378.6	236.8	23.9	92.9
p-value	<2.2E-16	3.91E-16	2.29E-08	6.42E-13
R^2	0.968	0.980	0.867	0.965

which will be analyzed later.

From Fig. 7a and Fig. 8a, it can be deduced that the bloating index is positively affected by a decrease in the proportion of kaolin, in favor of the addition of Fe_3O_4. This differs with what was observed in the previous study using pyrite, which in no case favored expansion [22]. Returning to this work, as the centroid of the kaolin is at 70 wt%, the effect plots (Fig. 8a) suggest that *BI* tends to increase particularly when K is between 40 and 70 wt%, especially in the 50–60 wt% range. In the case of magnetite, the centroid is at 25 wt% of M, so that the largest increases in *BI* occur when approximately 20 wt% of added iron phase is exceeded, especially between 25 and 45 wt%. Similarly, the increase in organic matter (cork powder) seems to have a positive effect on the increase in *BI*.

In the case of sodium carbonate, its incorporation in the mixtures implies a decrease in the expansive potential (in agreement with Bernhardt et al. [14] and the authors' previous investigation [22]), changing the trend somewhat from values above 2.5 wt%. However, it has been observed that the incorporation of Na_2CO_3 favors a greater sphericity in the LWA obtained (Fig. 9a), something that could be interesting when, for example, the aim is to use this LWA in a more workable concrete. Since the bloating effect seems to be less marked when Na_2CO_3 is added, a possible explanation is that Na_2CO_3 could promote the development of a more viscous and plastic shell, capable of better adapting to the pressure exerted by the increase in volume during bloating. This hypothesis agrees to some extent with the findings of Bernhardt et al. [14], who observed that the incorporation of Na_2CO_3 reduces the viscosity of the pellet surface during heating, which also favors the tendency of the specimens to stick together (something also observed in this research). However, in their case, the LWAs that contained this additive had more irregular shapes, something that is the opposite of what was seen in the present study, probably because Bernhardt et al. [14] excessively reduced the viscosity of the aggregate crust. On the contrary, the LWA shell without sodium carbonate would be more rigid when heated, so that the expansion will lead to the breakage of this external layer, favoring more the expansion through some areas than through others, thus producing a more irregular final shape of the aggregate (Fig. 9a).

Therefore, considering the four possible starting components of the formulations, the aggregate expansion process seems to be promoted when relatively high proportions of Fe_3O_4 are added to kaolin in the presence of organic carbon and absence of sodium carbonate. The structure of some highly expanded aggregates is shown in Fig. 9b,c, in which a very porous black core, surrounded by a thin reddish crust, can be seen. These changes in coloration and porosity are due to the following causes.

When introduced into the kiln, the surface of the pellet is in contact with the surrounding air, in which there is sufficient oxygen not only to decompose the organic components in the form of CO_2 and H_2O (g), but also to oxidize the magnetite according to the reaction:

$$4Fe_3O_4 + O_2 \rightarrow 6Fe_2O_3 \quad (3)$$

The formation of this Fe_2O_3 from Fe_3O_4 is responsible for the reddish color of the LWA shell, which is consistent, for example, with the neoformation of minerals such as hematite (Table 5). According to the DTA-TG test in air in Fig. 4b, this oxidation reaction is exothermic, starting at 275 °C (with a maximum at this temperature), and can gradually extend up to about 1000 °C [38], having in any case an associated weight increase as a consequence of the fixation of O_2 from the surrounding air.

On the contrary, inside the pellet there will be a deficit of oxygen due to the following causes: on the one hand, the O_2 may have difficulties to enter towards the inside due not only to the formation of the sintered outer shell, but also because it would have to flow against the gas stream released from the inside of the aggregate towards the outside (in fact, such a gas stream could even drag the internal O_2 outwards). On the other hand, the oxidation of the organic carbon of the cork and part of the Fe_3O_4 (see Eq. (3) will favor a rapid demand in the consumption of O_2 in the interior and the concomitant decrease in its concentration, thus producing incomplete oxidation reactions of the organic components, resulting in turn in the formation of CO with great reductive capacity. The interaction between this CO with both the oxidized (Fe_2O_3) and non-oxidized magnetite phases can lead to the following reactions in accordance with Park et al. [39] and Wie et al. [19]:

$$3Fe_2O_3 + CO \rightarrow 2Fe_3O_4 + CO_2 \quad (4)$$

$$Fe_2O_3 + CO \rightarrow 2FeO + CO_2 \quad (5)$$

$$2Fe_3O_4 + CO \rightarrow 3FeO + Fe_3O_4 + CO_2 \quad (6)$$

$$Fe_3O_4 + CO \rightarrow 3FeO + CO_2 \quad (7)$$

When the absence of oxygen is very marked, in such a case it could be the case that the unburned organic matter reacts directly with the Fe_2O_3 [17]:

$$Fe_2O_3 + C \rightarrow 2FeO + CO \quad (8)$$

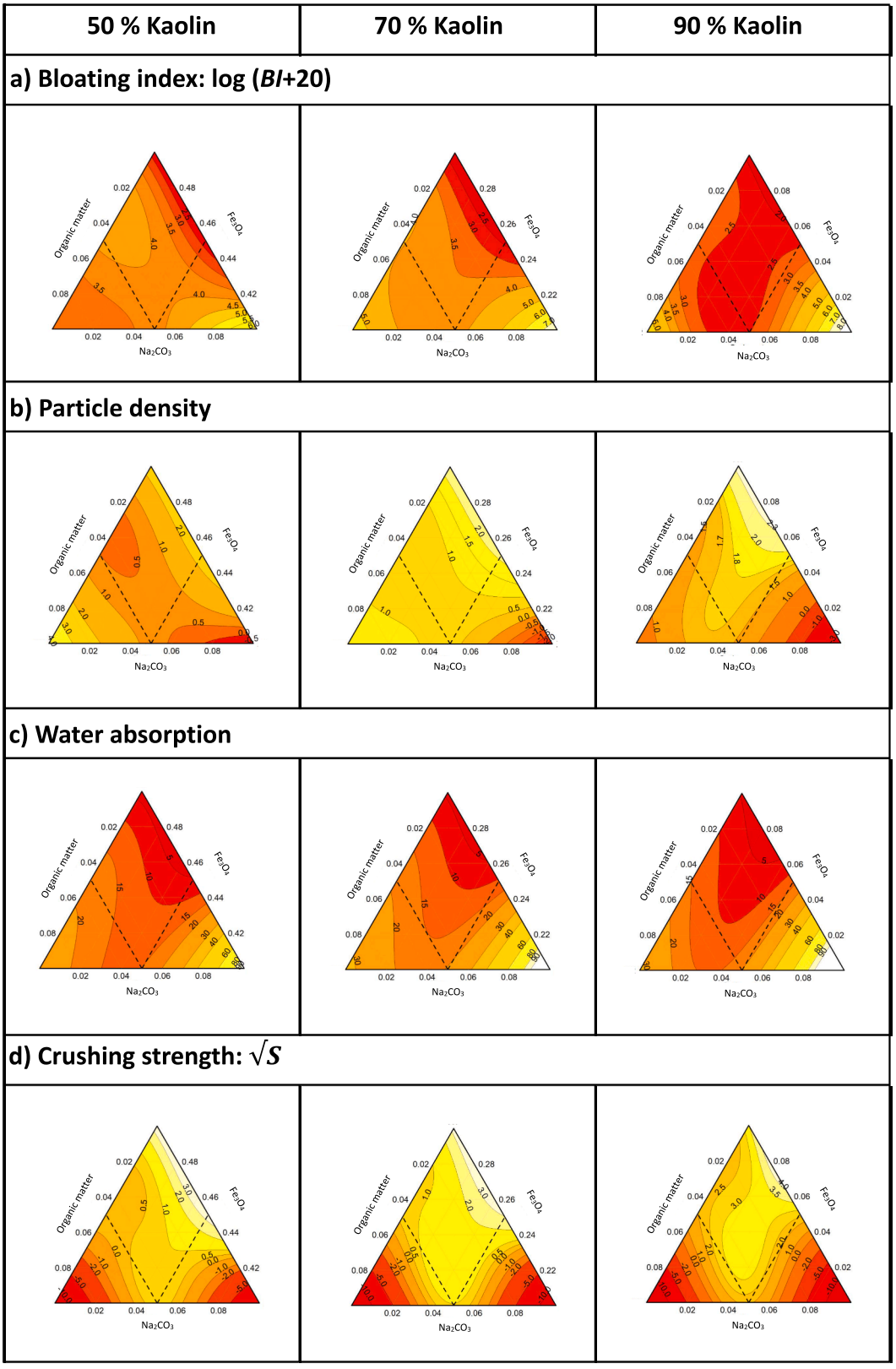

Fig. 7. Response surface plots for 50, 70 and 90 % kaolin: (a) bloating index according to log (BI + 20) model; (b) particle density; (c) water absorption; (d) crushing strength according to S square root model.

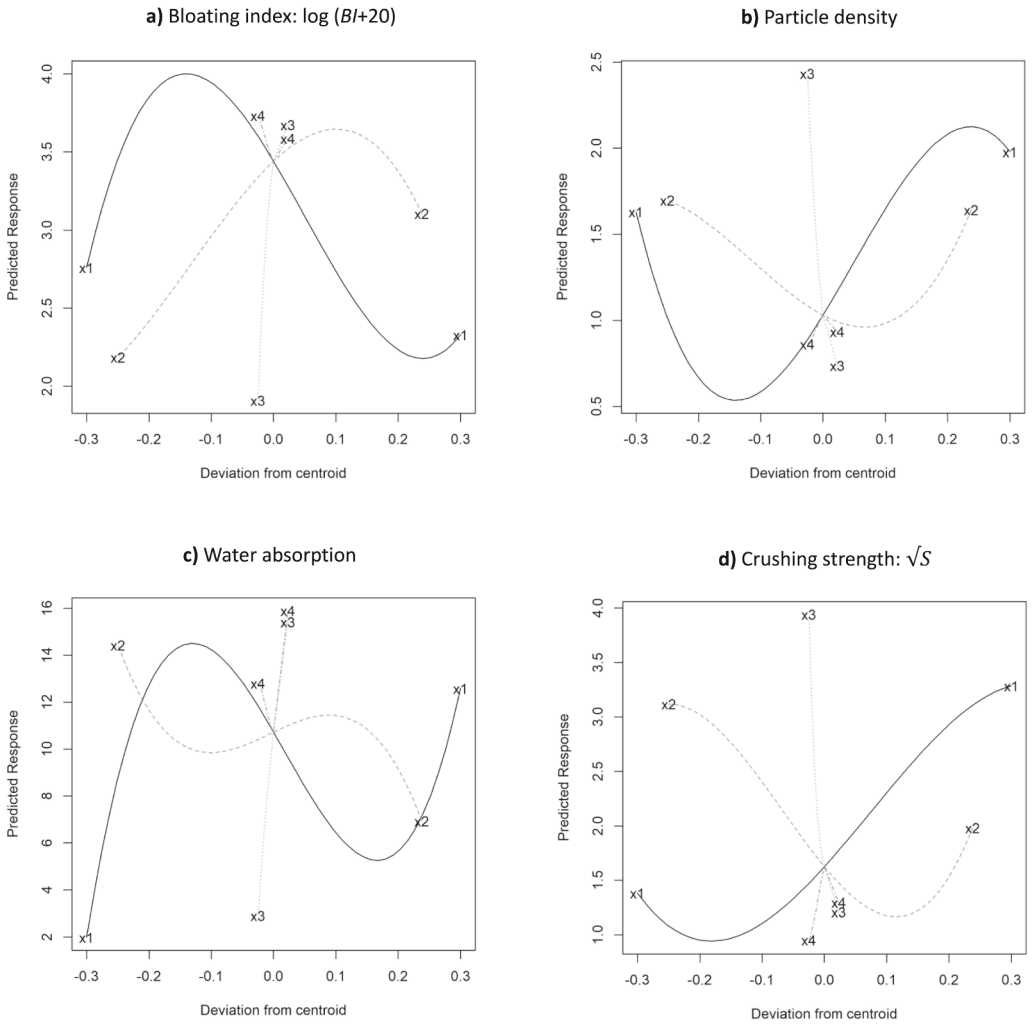

Fig. 8. Effect plots for: (a) bloating index according to log ($BI + 20$) model; (b) particle density; (c) water absorption; (d) crushing strength according to S square root model. Where: x1 = % kaolin; x2 = % Fe_3O_4; x3 = % organic matter (cork); x4 = % Na_2CO_3.

Considering the magnetite in this study, such a reaction could also occur as follows:

$$Fe_3O_4 + C \rightarrow 3FeO + CO \quad (9)$$

Similarly, as reported in Toyama and Kawamura [17], Fe_2O_3 in the aluminosilicate matrix loses its stability at high temperatures favoring the release of O_2 according to the following reaction:

$$2Fe_2O_3 \rightarrow 4FeO + O_2 \quad (10)$$

An intermediate reaction of the previous one is the following, which also results in the formation of FeO and oxygen:

$$2Fe_3O_4 \rightarrow 6FeO + O_2 \quad (11)$$

The reaction defined by Eq. (11) is, in theory, the responsible for the mass loss observed in Fig. 4d when the temperature exceeds 1050 °C in inert atmosphere. This concurs with the neoformation of minerals such as hercynite ($Fe^{2+}Al_2O_4$) (Table 5), which are generated due to the presence of reduced iron phases. Considering the molar masses of magnetite (231.5 g/mol), hercynite (125.8 g/mol), their corresponding iron contents (167.5 and 55.8 g/mol, respectively) and the fact that M25 formulation contained 37.5 wt% M (Table 1) with LOI of 14.5% (Table 3), it can be estimated that the LWA M25 holds 31.7 wt% of iron, of which 12.7 wt% is in crystalline form (hercynite), with the remaining 19 wt% being in the amorphous phase indicated in Table 5. Based on the various reactions shown above, the iron in the glassy phase is expected to be in the form of FeO.

According to the literature [5,6,17,19,40], the formation of reduced iron phases, such as FeO, are responsible for the development of the black core in the LWA and the suitable viscosity. FeO is a powerful flux capable of significantly lowering the melting point of the mineral matrix, which allows the development of a liquid phase (see the high amorphous content in Table 5) for trapping part of the gases formed (CO_2, CO, H_2O(g) and/or O_2 from the components of the present study formulations) thus generating a very porous expanded structure.

3.3.2. *Density and crushing strength modeling and their relation to LWA bloating*

As the effect plots of density and crushing strength show similar trends (Fig. 8b,d) they will be discussed together. In the case of oven-dry density (also called particle density), a cubic model has been used, which has not required any transformation since it was statistically well specified. For the crushing strength, S, the untransformed model had two problems. First, the contour plots showed negative values within the feasible region (which did not make physical sense). Second, the model was statistically misspecified. Taking these drawbacks into account, a Box-Cox transformation was performed, which determined that the best approach was to consider as independent variable the square root of S (hereinafter, $\sqrt{S}$), being the cubic model finally fitted.

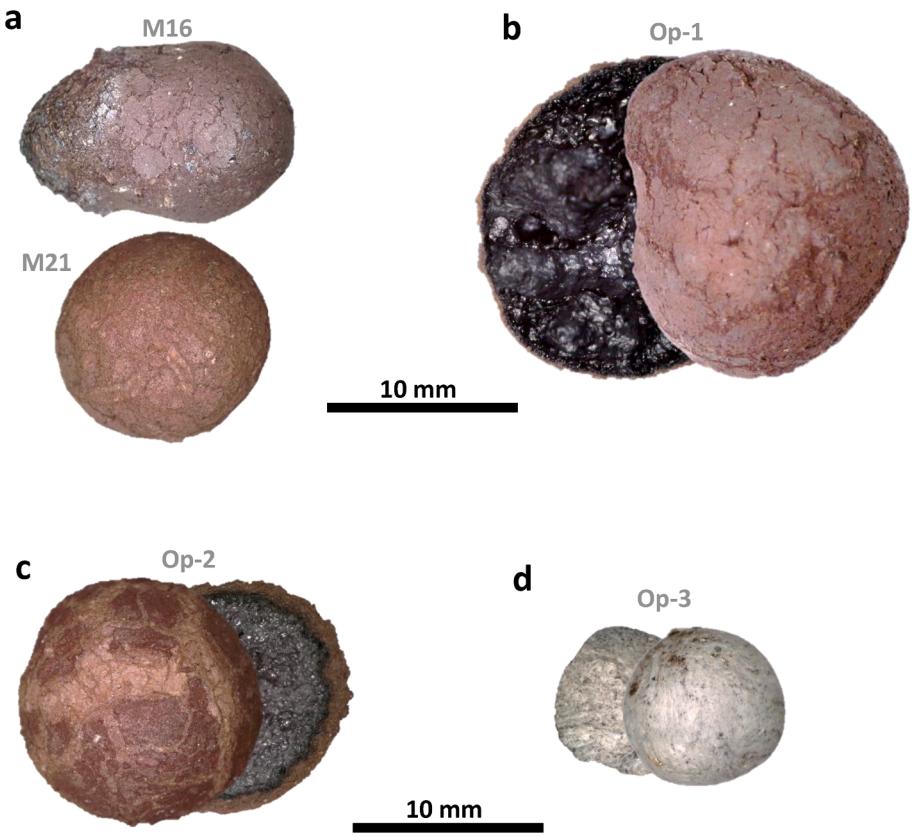

Fig. 9. Some selected aggregate specimens: (a) shape comparison between one LWA without sodium carbonate (M16) and one containing it (M21); (b) shell (red) and core (black) for the LWA corresponding to the Op-1 formulation; (c) shell (red) and core (gray) for the LWA corresponding to the Op-2 formulation; (d) exterior and interior of a specimen sintered from the Op-3 mixture. (For interpretation of the references to color in this figure legend, the reader is referred to the web version of this article.)

Table 5
Differentiation between shell and core mineralogy of the LWA sintered from the M25 blend.

	Amorphous	Mullite	Cristobalite	Pyroxene	Hematite	Magnetite	Hercynite
Shell	67.1	9.6	1.6	6.5	7	8.2	–
Core	71.5	–	–	–	–	–	28.5

The graphs in Fig. 7b and Fig. 8b for the density show that the behavior is essentially the same as that observed in the bloating index, only in this case with the opposite trend. In the case of mechanical strength (Fig. 7d and Fig. 8d), although the similarity is not as high, it can be seen that the trend also agrees to a large extent with that followed by aggregate density. Such behaviors are in line with expectations, since, as mentioned above, there is an inverse relationship between density and bloating index (Fig. 5c) and between mechanical strength and porosity (Fig. 5f) and, accordingly, also with *BI* (Fig. 5d). Therefore, for those percentage ranges of each component in which there is an increase in bloating index, there will be a decrease in density and crushing strength and vice versa, so that the discussion of the results is the same as indicated in the previous section.

3.3.3. *Water absorption modeling and factors involved*

The model applied for water absorption was also cubic and did not require any transformation either. The behavior of WA_{24} (Fig. 7c and Fig. 8c) is more complex than those previously observed for *BI* and ρ_{rd}. Thus, in the case of kaolin content, water absorption seems to be favored both when kaolin presents relatively low percentages (approx. between 50 and 70 wt%) as well as with percentages close to 100 wt% of clay. However, the kaolin trend presents a practically inverse relationship with respect to the Fe_3O_4 content, so that the maximum values of WA_{24} with respect to K are usually the minimum for magnetite and vice versa (Fig. 8c). This phenomenon means that the absorption seems to be favored in the absence of magnetite, or on the other hand, in percentages around 25–40 wt% of this mineral, which are usually those in which *BI* also increases and density decreases (Fig. 8a,b,c). For its part, the addition of cork does favor an increase in absorption as its percentage increases, while the addition of Na_2CO_3 also tends to increase it when exceeding 2.5 wt%.

These results suggest that two ways could coexist to favor water absorption, something that is also evident if the results of WA_{24} for the mixtures M4, M9, M10, M20, M22 and M25 are compared (Table 1 and Table 3). These six formulations present WA_{24} values in the same range (18–22%), however the first three have a high kaolin content and a low Fe_3O_4 proportion, which has resulted in the absence of volumetric expansion (the mineral matrix has not achieved the adequate viscosity for retaining gas) and a predominance of open porosity over closed porosity, fundamentally due to the voids left by the decomposition of cork and sodium carbonate. On the contrary, the LWAs developed from M20, M22 and M25 have between 25 wt% and 37.5 wt% of M in their formulation (Table 1), in addition to high *BI* and a predominance of closed porosity compared to open porosity (Table 3) because in this case an adequate viscous matrix has been developed to trap part of the gases released during the different thermo-chemical reactions that occur during firing. However, even presenting a relatively low ratio of open to closed pores, their volume is large in absolute terms, favoring high water absorption, as explained in Section 3.2.3 with reference to Fig. 5h.

3.4. Optimization of key properties and validation of models

Based on the data in Table 4, the optimal formulations (expressed in weight percentages) have been computed in order to obtain the maximum values of *BI*, WA_{24} and *S*, and the minimum ρ_{rd}. Such mixtures are shown in Table 6. For the bloating index and particle density, the optimum formulations were practically the same: 55.5% K + 40.7% M + 3.8% C + 0% N for the maximum estimated value of *BI* and 56.4% K + 39.6% M + 4.0% C + 0% N for the minimum estimated ρ_{rd}. After some preliminary tests, it was observed that the LWA specimens obtained by one mixture and the other were equal, so it was finally considered that the intermediate formulation (56.0% K + 40.2% M + 3.9% C + 0% N; see Op-1 in Table 6) was the one that best satisfied both properties together. The LWA obtained from this mixture is shown in Fig. 9b.

Regarding the optimum (maximum) of water absorption, this would correspond to the formulation Op-2 in Table 6: 66.1% K + 23.9% M + 5.0% C + 5.0% N and the specimen shown in Fig. 9c. For the theoretical maximum of *S*, the estimated formulation is 91.8% K + 5.6% M + 0% C + 2.6% N is the formulation (Op-3 in Table 6), with a selected specimen shown in Fig. 9d.

If the estimated values are compared with those obtained after testing the aggregates obtained from each optimum formulation, it can be seen that the two models with the worst estimate are those of WA_{24} and *S*. With respect to the former, the average difference in absolute value between the experimental and estimated values is >40%. Despite this, the water absorption difference is only one percentage point for the formulation Op-3 (WA_{24} exp. = 2.1% vs WA_{24} est. = 3.1%) and also relatively narrow for Op-2 (25.4% vs 21.0% of WA_{24}). However, the water absorption of the aggregates corresponding to the mixture Op-1 present a difference between the estimated and experimental data of 26.8 percentage points (59.7%). The result of WA_{24} obtained experimentally for this mixture (WA_{24} = 44.8%) has not only far exceeded the maximum estimated for this formulation (18%), but also that of Op-2 (21%) and even the maximum experimentally obtained in the previous tests (M25 = 22%; Table 3). These results indicate that the optimal formulation for maximizing water absorption coincides with that of the bloating index and density because the open pore volume per specimen is the largest of all possible according to the trend in Fig. 5h, an aspect that is also supported by the size and porosity of the sample depicted in Fig. 9b which outperform in this regard the mixture originally estimated to maximize WA_{24} (Fig. 9c).

Regarding the crushing strength results, in terms of percentage points, the differences are narrow between the experimental and optimum data for the Op-1 and Op-2 formulations, whose *S* value is very low (<1 MPa). However, in the formulation relative to the maximum mechanical strength (Op-3) the difference is 5.4 points (41.4%). Unlike what happened with the WA_{24} model for the samples with higher absorption capacity, the *S* model has overestimated its prediction (18.3 MPa vs. 12.9 MPa), so that a priori it seems to work better for the aggregates with lower mechanical strength (Op-1 and Op-2). In fact, the *S* results in Table 3 show six varieties (M3, M15, M17, M27, M29 and M33) of aggregates from those originally obtained that exceed the mechanical strength of Op-3. Those varieties of aggregate with higher mechanical strength have a much smaller size (shrinkage occurs instead of bloating) and a simple structure (no differentiation between shell and core), such as the specimen shown in Fig. 9d.

On the other hand, the data in Table 6 show that the particle density is generally well defined for the aggregates obtained from the Op-2 and Op-3 formulations. The largest difference observed is for the Op-1 formulation (28.1%), although, in absolute terms it is only 0.09 g/cm^3, which reveals that the density model predicts quite accurately. The minimum density estimated (and experimentally recorded) is therefore that of Op-1 (0.32 g/cm^3), coinciding with the fact that it is the LWA variety with the highest bloating index (*BI* exp. = 62.6%). This experimental result is very close to the estimated one (*BI* est. = 66.5%), implying a difference of only 3.9 percentage points (6.2%). These

Table 6
Optimal formulations and comparison between experimentally determined and statistically model-estimated properties.

		Bloating index (%)			Particle density (g/cm^3)				Water absorption (%)				Crushing strength (MPa)			
Optimum formulation	Exp.	Est.	Dif.	Dif. %	Exp.	Est.	Dif.	Dif. %	Exp.	Est.	Dif.	Dif. %	Exp.	Est.	Dif.	Dif. %
Op-1 (for max *BI* and min ρ_{rd})	56.0% K + 40.2% M + 3.9% C + 0% N	62.6	66.5	3.9	6.2	0.32	0.23	−0.09	−28.1	44.8	18.0	−26.8	−59.7	0.1	0.0	0.0
Op-2 (for max WA_{24})	66.1% K + 23.9% M + 5.0% C + 5.0% N	33.4	31.4	−2.0	−5.8	0.50	0.57	0.07	14.0	25.4	21.0	−4.5	−17.5	0.9	0.6	−0.3	−32.6
Op-3 (for max *S*)	91.8% K + 5.6% M + 0% C + 2.6% N	−14.0	−13.8	0.3	−1.9	2.37	2.37	0.00	−0.2	2.1	3.1	1.0	48.6	12.9	18.3	5.4	41.4
				|Mean|	4.6			|Mean|	14.1			|Mean|	41.9			|Mean|	24.7

differences between the estimated and experimental *BI* values are even smaller in Op-2 and Op-3 (Table 6), which shows that the model used to estimate this parameter works very well. This is especially relevant, since the expansive potential of a formulation intended for the manufacture of lightweight aggregates is the fundamental and most revealing parameter of all, since from it one can practically deduce the rest of the technological properties, as could be discussed on the basis of the graphs in Fig. 5.

The Op-1 mixture (Table 6, Fig. 9b) therefore confirms that a highly refractory clay (such as the kaolin in this study) with low flux content (Table 2) requires the incorporation of relatively large amounts of Fe_3O_4 (40%) along with the addition of a small amount of organic matter (4%) to maximize its bloating capacity.

3.5. Opportunities for industrial scale-up and sustainability of the process

Considering the materials used and the results obtained, it is essential to understand whether they have industrial applicability and, if so, whether the process is sustainable. Regarding the use of a kaolin clay free of organic matter, Na_2CO_3, and negligible amounts of iron (0.4%), it has been necessary from a theoretical point of view to understand how these three additives affect the development of expanded lightweight aggregates (it is worth remembering that the first main goal of this research is to unravel the synergistic processes involved in the formation of LWAs from "ideal" components based on a fundamentally scientific vision).

Beyond this, kaolin is a very abundant and low-cost clay, which makes it accessible if the process is to be reproduced at an industrial level. However, the fact that it is a natural raw material might seem, a priori, to detract from its environmental value. In this sense, it is important to point out that the production of LWAs can be carried out using other types of aluminosilicate sources, such as waste clays [11], so there would be no inconvenience in implementing the process with totally sustainable raw materials.

In line with the above, the results shown in section 3.4 show that the proportion of Fe_3O_4 is very high to achieve the maximum bloating and minimum density (40 wt%), which could in principle be a handicap if the aim is to scale up the process to an industrial level. However, this work is part of a larger project whose main objective is the recovery of metal mining wastes (very abundant worldwide) to recycle them as raw materials in the manufacture of lightweight aggregates at an industrial level, thus reducing economic and environmental costs.

In addition, the use of a residue such as cork powder also adds environmental value to the manufacturing process. Its effectiveness in combination with the iron component to form the porous structure would not only be attributable to cork, but could also be achieved through other organic wastes [13]. This would facilitate that, in case of a potential industrial scale-up, manufacturers can adapt to the organic waste that suits them best.

From an operational point of view, the manufacturing process of lightweight aggregates requires high temperatures (between 1135 and 1345 °C in this work). Despite this, it has been shown that the incorporation of the additives studied, M, C and N, can lead to a notable drop in the working temperature (section 3.2.1; Table 1 and Table 3), thus reducing the energy consumption required for its production. In addition, it must be considered that, unlike other ceramic materials (for example, bricks), LWA is fired for much shorter times (minutes versus hours) and that, in addition, its increase in volume (bloating) allows a larger quantity of product from the same amount of starting clay to be obtained. This higher performance makes lightweight aggregate an industrially profitable and sustainable material.

Therefore, the approaches developed in this investigation will serve as a basis to facilitate an engineering strategy applicable to the aforementioned industrial scaling using waste.

4. Conclusions

Based on the findings shown in the previous sections of this article, the following conclusions can be drawn:

The bloating process in LWA and its associated decrease in density from non-self-expanding kaolin has required the addition of Fe_3O_4 (M) in combination with an organic component (in this study cork powder, C). The incorporation of one of these phases without the other or with an inadequate amount of it does not generate the desired effect. Thanks to the action of C as a reducing agent, FeO can be formed in the core leading to an adequate viscosity in the mineral matrix to trap the gases involved in pore formation.

The incorporation of Na_2CO_3 has favored the development of a more spherical shape in those specimens that initially contained this component. A possible explanation for this phenomenon is that Na_2CO_3 could promote the development of a more viscous and plastic shell, capable of better adapting to the pressure exerted by the increase in volume during bloating.

Two antagonistic mechanisms could be involved in increasing water absorption capacity. On the one hand, WA_{24} is enhanced through the development of non-expanded aggregates in which the pores generated come fundamentally from the voids left by the thermal decomposition of organic carbon and/or minerals such as carbonates. The second mechanism is the development of a highly expanded structure with a high proportion of closed pores, but in which, however, the open pores have a relevant volume to act as water reservoirs. This second route has been the one that has resulted in the greatest absorption of water (WA_{24} = 44.8%), through the most expanded (*BI* = 62.6%) and lightest (ρ_{rd} = 0.32 g/cm^3) LWA, whose formulation has been: 56.0% kaolin + 40.2% Fe_3O_4 + 3.9% C + 0% Na_2CO_3.

In the case of crushing strength, as expected, it decreases as the porosity and lightness of the aggregate increases. Therefore, if the objective is to obtain synthetic aggregates with high mechanical strength, it is critical to avoid the incorporation of certain components (such as organic carbon) that could trigger the expansive process.

The models obtained through the ME-DOE statistical method have been generally satisfactory to understand the synergies between the different components of the mixtures and to optimize the bloating index, density, water absorption and crushing strength. The resulting formulations have presented a good degree of fit between the experimental and estimated data, especially for *BI* and ρ_{rd}.

These results confirm that statistical methods could have great potential to obtain basic knowledge of the processes involved (scientific perspective), as well as bespoke solutions through tailor-made mixtures based on the desired technological requirements (engineering perspective, applicable to industry). In this sense, the "theoretical" approaches developed in this research will serve as a basis to facilitate an industrial scale-up. This aspect would be part of a broader research, whose objective will be the use of metal mining wastes as raw materials, which are abundant worldwide, thus saving economic costs and solving an environmental problem.

Declaration of Competing Interest

The authors declare that they have no known competing financial interests or personal relationships that could have appeared to influence the work reported in this paper.

Data availability

Data will be made available on request.

Acknowledgments

This research was conducted as a part of the ECO-MET-AL Project, PID2019-109520RB-I00 / AEI / 10.13039/501100011033, "Can

industrial and mining metalliferous wastes produce green lightweight aggregates? Applying the Circular Economy" funded by the Spanish Ministry of Science, Innovation and Universities and ERDF funds, framed in the "Ayudas a "Proyectos I + D + i" en el marco de los Programas Estatales de Generación de Conocimiento y Fortalecimiento Científico y Tecnológico del Sistema de I + D + i y de I + D + i orientada a los Retos de la Sociedad, Convocatoria 2019". Thanks also to the SCAI of the University of Jaén (Spain), the University of Castilla-La Mancha (Spain) and the University of Málaga (Spain) for their services.

References

[1] ANEFA, 2022. El sector (The aggregate sector in Spain). Asociación Nacional de Empresarios Fabricantes de Áridos. http://www.aridos.org/el-sector/ (accessed in June 2022).
[2] ESCSI, 2022. Expanded Shale, Clay and Slate Institute. https://www.escsi.org/ (accessed in June 2022).
[3] En-13055-1,, Lightweight aggregates. Part 1: Lightweight aggregates for concrete, mortar and grout, European Committee for Standardization, 2002.
[4] B. Ayati, V. Ferrándiz-Mas, D. Newport, C. Cheeseman, Use of clay in the manufacture of lightweight aggregate, Constr. Build. Mater. 162 (2018) 124–131, https://doi.org/10.1016/j.conbuildmat.2017.12.018.
[5] J.M. Moreno-Maroto, C.J. Cobo-Ceacero, M. Uceda-Rodríguez, T. Cotes-Palomino, C. Martínez García, J. Alonso-Azcárate, Unraveling the expansion mechanism in lightweight aggregates: Demonstrating that bloating barely requires gas, Constr. Build. Mater. 247 (2020) 118583.
[6] C.M. Riley, Relation of chemical properties to the bloating of clays, J. Am. Ceram. Soc. 34 (4) (1951) 121–128, https://doi.org/10.1111/j.1151-2916.1951.tb11619.x.
[7] E.G. Ehlers, The Mechanism of Lightweight Aggregate Formation, Am. Ceram. Soc. Bull. 37 (2) (1958) 95–99.
[8] J.C. Cubaud, M. Murat, Fabricación industrial de arcilla expandida, Silicates Industriels 19 (133) (1969) 5–16.
[9] G. Cougny, Specifications for clayey raw materials used to produce expanded lightweight aggregates, Bull. Int. Assoc. Eng. Geol. 41 (1990) 47–55, https://doi.org/10.1007/BF02590206.
[10] J. Decleer, W. Viaene, Rupelian Boom clay as raw material for expanded clay manufacturing, Appl. Clay Sci. 8 (1993) 111–128, https://doi.org/10.1016/0169-1317(93)90032-V.
[11] M. Dondi, P. Cappelletti, M. D'Amore, R. de Gennaro, S.F. Graziano, A. Langella, M. Raimondo, C. Zanelli, Lightweight aggregates from waste materials: Reappraisal of expansion behavior and prediction schemes for bloating, Constr. Build. Mater. 127 (2016) 394–409, https://doi.org/10.1016/j.conbuildmat.2016.09.111.
[12] J.M. Moreno-Maroto, M. Uceda-Rodríguez, C.J. Cobo-Ceacero, M. Calero de Hoces, M.A. Martín Lara, T. Cotes-Palomino, A.B. López García, C. Martínez-García, Recycling of 'alperujo' (olive pomace) as a key component in the sintering of lightweight aggregates, J. Cleaner Prod. 239 (118041) (2019), https://doi.org/10.1016/j.jclepro.2019.118041.
[13] C.J. Cobo-Ceacero, J.M. Moreno-Maroto, M. Guerrero-Martínez, M. Uceda-Rodríguez, A.B. López, C. Martínez García, T. Cotes-Palomino, Effect of the addition of organic wastes (cork powder, nut shell, coffee grounds and paper sludge) in clays to obtain lightweight aggregates, Bol. Soc. Esp. Ceram. Vidrio. 62 (1) (2022) 88–105, https://doi.org/10.1016/j.bsecv.2022.02.007.
[14] M. Bernhardt, H. Justnes, H. Tellesbø, K. Wiik, The effect of additives on the properties of lightweight aggregates produced from clay, Cem. Concr. Compos. 53 (2014) 233–238, https://doi.org/10.1016/j.cemconcomp.2014.07.005.
[15] Y. Ren, Q. Ren, Z. Huo, X. Wu, J. Zheng, O. Hai, Preparation of glass shell fly ash-clay based lightweight aggregate with low water absorption by using sodium carbonate solution as binder, Mater. Chem. Phys. 256 (2020), 123606, https://doi.org/10.1016/j.matchemphys.2020.123606.
[16] C.Y. Chien, K.Y. Show, C. Huang, Y.J. Chang, D.J. Lee, Effects of sodium salt additive to produce ultra lightweight aggregates from industrial sludge-marine clay mix: Laboratory trials, J. Taiwan Inst. Chem. Eng. 111 (2020) 105–109, https://doi.org/10.1016/j.jtice.2020.04.018.
[17] S. Toyama, M. Kawamura, On the relationship between the bloating of lightweight aggregate and reaction progress of the constituents, J. Chem. Eng. Jpn. 4 (3) (1971) 251–256.
[18] F. Sandrolini, C. Palmonari, Role of iron oxides in the bloating of vitrified ceramic materials, Trans. J. Brit. Ceram. Soc. 75 (2) (1976) 25–32.
[19] Y.M. Wie, K.G. Lee, K.H. Lee, Chemical design of lightweight aggregate to prevent adhesion at bloating activation temperature, J, Journal of Asian Ceramic Societies 8 (2) (2020) 245–254.
[20] Y.L. Wei, J.C. Jang, K.W. Ko, Evidence for a new mechanism of Fe_2O_3 decomposition in lightweight aggregate formation, Environ. Chem. Lett. 10 (2012) 41–47, https://doi.org/10.1007/s10311-011-0326-2.
[21] Y.L. Wei, Y.Y. Lin, Role of Fe compounds in light aggregate formation from a reservoir sediment, J. Hazard. Mater. 171 (2009) 111–115, https://doi.org/10.1016/j.jhazmat.2009.05.122.
[22] J.M. Moreno-Maroto, C.J. Cobo-Ceacero, A. Conde-Sánchez, A.M. Martínez-Rodríguez, B. González-Corrochano, J. Alonso-Azcárate, M. Uceda-Rodríguez, A. B. López, C. Martínez-García, T. Cotes-Palomino, Can statistical methods optimize complex multicomponent mixtures for sintering ceramic granular materials? Ceramics International 49 (14) (2023) 24195–24206.
[23] J. Cornell, Experiments with Mixtures, (3rd ed.), John Wiley & Sons, New York, 2002.
[24] J. Lawson, C. Willden, Mixture Experiments in R Using mixexp, Journal of Statistical Software, Code Snippets 72 (2) (2016) 1–20, https://doi.org/10.18637/jss.v072.c02.
[25] ASTM D 4318–10e1,, Standard Test Methods for Liquid Limit, Plastic Limit, and Plasticity Index of Soils, Annual Book of ASTM Standards, ASTM International, West Conshohocken, PA, 2017.
[26] J.M. Moreno-Maroto, J. Alonso-Azcárate, Plastic Limit and Other Consistency Parameters by a Bending Method and Interpretation of Plasticity Classification in Soils, Geotech. Test. J. 40 (3) (2017) 467–482, https://doi.org/10.1520/GTJ20160059.
[27] E. Fakhfakh, W. Hajjaji, M. Medhioub, F. Rocha, A. López-Galindo, M. Setti, F. Kooli, F. Zargouni, F. Jamoussi, Effects of sand addition on production of lightweight aggregates from tunisian smectite-rich clayey rocks, Appl. Clay Sci. 35 (2007) 228–237, https://doi.org/10.1016/j.clay.2006.09.006.
[28] En-1097-3,, Tests for mechanical and physical properties of aggregates. Part 3: Determination of loose bulk density and voids, European Committee for Standardization, 1998.
[29] En-1097-6,, Tests for mechanical and physical properties of aggregates. Part 6: Determination of particle density and water absorption, European Committee for Standardization, 2013.
[30] Aci 213r–03,, Guide for Structural Lightweight-Aggregate Concrete, American Concrete Institute, 2003.
[31] Y. Ke, A.L. Beaucour, S. Ortola, H. Dumontet, R. Cabrillac, Influence of volume fraction and characteristics of lightweight aggregates on the mechanical properties of concrete, Constr. Build. Mater. 23 (8) (2009) 2821–2828, https://doi.org/10.1016/j.conbuildmat.2009.02.038.
[32] C. De Santiago Buey, M. Raya García, Análisis del peso específico y porosidad de materiales porosos mediante picnometría de helio, Ing. Civil 151 (2008) 95–103. ISSN 0213–8468.
[33] M. Bernhardt, H. Tellesbø, H. Justnes, K. Wiik, Mechanical properties of lightweight aggregates, J. Eur. Ceram. Soc. 33 (2013) 2731–2743, https://doi.org/10.1016/j.jeurceramsoc.2013.05.013.
[34] S. Yashima, Y. Kanda, S. Sano, Relationship between particle size and fracture energy or impact velocity required to fracture as estimated from single particle crushing, Powder Technol. 51 (1987) 277–282.
[35] Y. Li, D. Wu, J. Zhang, L. Chang, D. Wu, Z. Fang, Y. Shi, Measurement and statistics of single pellet mechanical strength of differently shaped catalysts, Powder Technol. 113 (1-2) (2000) 176–184.
[36] J.M. Moreno-Maroto, B. González-Corrochano, J. Alonso-Azcárate, L. Rodríguez, A. Acosta, Assessment of crystalline phase changes and glass formation by Rietveld-XRD method on ceramic lightweight aggregates sintered from mineral and polymeric wastes, Ceram. Int. 44 (2018) 11840–11851, https://doi.org/10.1016/j.ceramint.2018.03.274.
[37] J.M. Moreno-Maroto, J. Alonso-Azcárate, What is clay? A new definition of "clay" based on plasticity and its impact on the most widespread soil classification systems, Appl. Clay Sci. 161 (2018) 57–63, https://doi.org/10.1016/j.clay.2018.04.011.
[38] Földvári, M., 2011. Handbook of thermogravimetric system of minerals and its use in geological practice. Occasional Papers of the Geological Institute of Hungary. Geological Institute of Hungary. Vol. 213. ISBN:978-963-671-288-4.
[39] J.Y. Park, Y.T. Kim, K.G. Lee, S. Kang, J.H. Kim, The mechanism of black core formation, J. Kor. Cryst Growth Cryst. Tech. 15 (5) (2005) 208–215.
[40] K.G. Lee, Bloating Mechanism of Lightweight Aggregate with the Size, J. Korean Ceram. Soc. 53 (2) (2016) 241–245, https://doi.org/10.4191/kcers.2016.53.2.241.